

ARTICLE

Cannabidiol inhibits the skeletal muscle Nav1.4 by blocking its pore and by altering membrane elasticity

Mohammad-Reza Ghovanloo^{1,2,3} , Koushik Choudhury^{3*}, Tagore S. Bandaru^{3*} , Mohamed A. Fouda^{1,4*} , Kaveh Rayani^{1*} , Radda Rusinova⁵ , Tejas Phaterpekar⁶, Karen Nelkenbrecher², Abeline R. Watkins¹, Damon Poburko¹ , Jenifer Thewalt⁶ , Olaf S. Andersen⁵ , Lucie Delemotte³ , Samuel J. Goodchild², and Peter C. Ruben¹ 

Cannabidiol (CBD) is the primary nonpsychotropic phytocannabinoid found in *Cannabis sativa*, which has been proposed to be therapeutic against many conditions, including muscle spasms. Among its putative targets are voltage-gated sodium channels (Navs), which have been implicated in many conditions. We investigated the effects of CBD on Nav1.4, the skeletal muscle Nav subtype. We explored direct effects, involving physical block of the Nav pore, as well as indirect effects, involving modulation of membrane elasticity that contributes to Nav inhibition. MD simulations revealed CBD's localization inside the membrane and effects on bilayer properties. Nuclear magnetic resonance (NMR) confirmed these results, showing CBD localizing below membrane headgroups. To determine the functional implications of these findings, we used a gramicidin-based fluorescence assay to show that CBD alters membrane elasticity or thickness, which could alter Nav function through bilayer-mediated regulation. Site-directed mutagenesis in the vicinity of the Nav1.4 pore revealed that removing the local anesthetic binding site with F1586A reduces the block of I_{Na} by CBD. Altering the fenestrations in the bilayer-spanning domain with Nav1.4-WWWW blocked CBD access from the membrane into the Nav1.4 pore (as judged by MD). The stabilization of inactivation, however, persisted in WWWW, which we ascribe to CBD-induced changes in membrane elasticity. To investigate the potential therapeutic value of CBD against Nav1.4 channelopathies, we used a pathogenic Nav1.4 variant, P1158S, which causes myotonia and periodic paralysis. CBD reduces excitability in both wild-type and the P1158S variant. Our *in vitro* and *in silico* results suggest that CBD may have therapeutic value against Nav1.4 hyperexcitability.

Introduction

The cannabis plant, *Cannabis sativa*, contains over 120 active constituents, collectively known as phytocannabinoids (Morales et al., 2017). Some phytocannabinoids mediate psychotropic effects; others do not (Morales et al., 2017). The primary nonpsychotropic phytocannabinoid is cannabidiol (CBD). The structure of CBD is nearly identical to the main psychotropic compound isolated from cannabis, Δ^9 -tetrahydrocannabinol (THC; Morales et al., 2017). The only structural difference between the two isomers is the presence of a free hydroxyl in CBD in place of a closed ring in THC. This structural difference underlies THC's high affinity for the human cannabinoid receptors, CB1 and CB2, which are thought to mediate the euphoria associated with using cannabis (Devinsky et al., 2017). In contrast to THC, CBD has little to no affinity for CB receptors (Pertwee, 2008), and CBD is suggested to be a negative allosteric modulator of CB1 receptors (CBD interactions with the CB1 orthosteric

site are of low affinity, but its allosteric modulation of CB1 is higher in affinity; Tham et al., 2019). However, CBD has been suggested to be a potentially therapeutic compound against a variety of conditions, including muscle spasms, pain, and seizures. Some reports of CBD's efficacy are anecdotal, whereas others have been experimentally and clinically substantiated (Devinsky et al., 2017). CBD showed therapeutic efficacy in a recent phase III human clinical trial against Dravet and Lennox-Gastaut syndromes (Devinsky et al., 2017, 2018), severe forms of childhood epilepsy, and it has received U.S. Food and Drug Administration approval for the nonseizure and quality-of-life management of these conditions.

Reports of CBD's efficacy, along with its low affinity for CB receptors, have inspired studies on its CB-independent actions. Many mechanisms and targets have been proposed for the action of CBD (Kaplan et al., 2017; Ghovanloo et al., 2018c; Ross

¹Department of Biomedical Physiology and Kinesiology, Simon Fraser University, Burnaby, BC, Canada; ²Department of Cellular and Molecular Biology, Xenon Pharmaceuticals, Burnaby, BC, Canada; ³Science for Life Laboratory, Department of Physics, Royal Institute of Technology, Solna, Sweden; ⁴Department of Pharmacology and Toxicology, Alexandria University, Alexandria, Egypt; ⁵Department of Physiology and Biophysics, Weill Cornell Medicine, New York, NY; ⁶Department of Molecular Biology and Biochemistry/Physics, Simon Fraser University, Burnaby, BC, Canada.

*K. Choudhury, T.S. Bandaru, M.A. Fouda, and K. Rayani contributed equally to this paper; Correspondence to Peter C. Ruben: pruben@sfu.ca.

© 2021 Ghovanloo et al. This article is distributed under the terms of an Attribution–Noncommercial–Share Alike–No Mirror Sites license for the first six months after the publication date (see <http://www.rupress.org/terms/>). After six months it is available under a Creative Commons License (Attribution–Noncommercial–Share Alike 4.0 International license, as described at <https://creativecommons.org/licenses/by-nc-sa/4.0/>).

et al., 2008; De Petrocellis et al., 2011; Patel et al., 2016; Sait et al., 2020). The voltage-gated sodium channel (Nav) family is among the suggested targets (Patel et al., 2016; Ghovanloo et al., 2018c), in part because Navs underpin many of the conditions for which CBD has been shown, or suggested, to be efficacious.

Sodium currents through Navs initiate action potentials (APs) in neurons, the myocardium, and skeletal muscles. Navs are heteromultimeric proteins composed of a large ion-conducting and voltage-sensing α -subunit and smaller β -subunits (Catterall, 2012; Ghovanloo et al., 2016; Ghovanloo and Ruben, 2020; Fouda et al., 2020). The α -subunit is a single transcript that includes four six-transmembrane-segment domains. Each domain can be divided into two functional subdomains: the voltage-sensing domain (VSD) and the pore-domain (Ghovanloo et al., 2016). These functional subdomains are connected through the intracellular S4-S5 linker (Yarov-Yarovoy et al., 2012). The Nav pore is the site of interaction for many pharmacological blockers (Lee et al., 2012; Gamal El-Din et al., 2018). The pore has four intra-bilayer fenestrations that connect it to the bilayer core; their functional roles remain speculative (Pan et al., 2018).

Disorders of the Nav subtype predominantly expressed in skeletal muscles, Nav1.4, are associated with contractility dysfunction. Nav1.4 normally generates the propagated AP that synchronizes the muscle contraction. Nav1.4 variants with disrupted gating may cause aberrant depolarization that can result in either hyper- or hypoexcitability (Cannon, 2006). Hyperexcitable (gain-of-function [GOF]) muscle channelopathies are classified as either nondystrophic myotonias or periodic paralyses (Lehmann-Horn et al., 2008). Most of these channelopathies arise from sporadic de novo or autosomal dominant mutations in SCN4A (Ghovanloo et al., 2018a).

The majority of GOF Nav1.4 variants result in myotonic syndromes, which are defined by a delayed relaxation after muscle contraction (Lehmann-Horn and Rüdell, 1995; Tan et al., 2011). There is an increase in muscle membrane excitability in which even a brief voluntary contraction can lead to a series of APs that may persist for several seconds after motor neuron activity is terminated, a condition that is perceived as muscle stiffness (Tan et al., 2011). These conditions are not considered lethal but can be life limiting due to the multitude of problems they can cause, including stiffness and pain (Vicart et al., 2005).

A cationic leak (gating-pore current in the VSD) with characteristics similar to the ω -current in *Shaker* potassium channels has been shown to cause periodic paralyses (Jiang et al., 2018; Tombola et al., 2005). This mechanism indicates that periodic paralyses can be caused by a severe form of GOF in Nav1.4 (Wu et al., 2011; Jiang et al., 2018). A subset of periodic paralyses is triggered by low serum $[K^+]$ and results in episodes of extreme muscle weakness. These are known as hypokalemic periodic paralyses (hypoPP; Miller et al., 2004). A serum $[K^+] < 3$ mM (normal concentration, 3.5–5.0 mM) may trigger hypoPP (Fontaine, 2008).

There are few therapeutic options for these skeletal muscle dysfunctions (considered rare conditions; Emery, 1991), and the treatment mostly relies on drugs developed for other conditions, including local anesthetics (LAs). Myotonia treatment is focused on reducing the involuntary AP bursts (Vicart et al., 2005; Desaphy et al., 2004); hypoPP treatment is focused mostly on

restoring serum $[K^+]$ (Torres et al., 1981; Tawil et al., 2000; Sternberg et al., 2001; Venance et al., 2004). Thus, there remains a need for drugs that alleviate the hyperexcitability associated with both myotonia and hypoPP. In this context, noneuphoric plant cannabinoids have been shown to enhance muscle quality and performance in dystrophic mdx mice (Iannotti et al., 2019), a finding we explore further in this study.

We first delineate the effects of CBD on Nav1.4, building on our previous description of the inhibitory effects of CBD on some neuronal Nav subtypes (Ghovanloo et al., 2018c). These findings prompted us to propose a mechanism by which CBD could inhibit Navs by both direct (direct/binding interactions with channel) and indirect (membrane-mediated) mechanisms. Specifically, we explored whether CBD accumulates in the membrane, which could alter membrane elasticity and, while residing in the membrane, might enter the Nav1.4 fenestrations and block the channel pore/alter channel gating (Gamal El-Din et al., 2018; Hille, 1977). Next, we explored the effects of CBD on a mixed periodic paralysis and myotonia Nav1.4 mutation (P1158S; Webb and Cannon, 2008; Ghovanloo et al., 2018a) to determine whether it could alleviate the mutant phenotypes. Our results suggest that CBD may alleviate the myotonic phenotype (and possibly, to a lesser extent, the periodic paralysis) associated with P1158S. Finally, we sought to survey whether saturating levels of CBD can reduce skeletal muscle contractility, which they do.

Materials and methods

Rat diaphragm preparation

Four 4-wk-old male Sprague Dawley rats (Charles River) were euthanized. The rat phrenic hemidiaphragm preparation was isolated according to the method described by Büllbring (1946). A fan-shaped muscle with an intact phrenic nerve was isolated from the left side and transferred to a container with Krebs solution (in mM: 95.5 NaCl, 4.69 KCl, 2.6 CaCl₂, 1.18 MgSO₄·7H₂O, 2.2 KH₂PO₄, 24.9 NaHCO₃, and 10.6 glucose) and aerated with carbogen (95% oxygen and 5% carbon dioxide). All experimental protocols were approved by the animal care and use committees. The contraction experiment was performed using a Radnoti Myograph system.

Molecular docking

Docking of CBD into the cryo-EM structure of human Nav1.4 (hNav1.4; Protein Data Bank [PDB] accession no. 6AGF) was performed using AutoDock Vina (Trott and Olson, 2010). CBD was downloaded in PDB format from DrugBank (Wishart et al., 2018), and searching of the conformational space allowed the sampling of all rotatable bonds. To dock CBD into Nav1.4, a large search volume of 82 Å × 100 Å × 82 Å was considered, which enclosed nearly the whole of the pore domain and parts of the VSD. This yielded the top nine best binding poses of CBD ranked by mean energy score. The top three poses are shown in Fig. S2.

MD simulation system preparation

We ran two different sets of MD simulations, the first consisting of CBD interacting with model 1-palmitoyl-2-oleoyl-sn-glycero-3-phosphocholine (POPC) membranes and the second consisting

of CBD interacting with the hNav1.4 channel embedded in its POPC/solution environment.

First, a homogeneous lipid bilayer consisting of 188 POPC molecules was prepared using the CHARMM-GUI Membrane Builder (Jo et al., 2008; Lee et al., 2016; Wu et al., 2014). Three different systems were created: one with two CBD molecules, each one placed in each leaflet of the bilayer (system 1); one with three CBDs, all of them placed in the upper leaflet (system 2); and one with six CBDs, of which three were placed in the upper leaflet and three in the lower leaflet (system 3). CBD was placed manually into the bilayer, with the polar headgroup of CBD facing the lipid headgroups. Lipid molecules with at least one atom within 2 Å of a CBD were manually deleted. A control simulation without any CBD was also prepared (system 0). The system was hydrated by adding two ~25 Å layers of water to both sides of the membrane. Last, 150 mM NaCl was added (30 Na⁺ and 30 Cl⁻). The simulation systems are summarized in Table S2. This system was defined as the lipid-CBD condition.

Second, hNav1.4 and the best docked position of CBD obtained from AutoDock Vina was used as a starting structure. The starting system was embedded into the POPC lipid bilayer. The system was hydrated by adding two ~25 Å layers of water to both sides of the membrane. Last, the system was ionized with 150 mM NaCl. This system is defined as the Nav1.4-CBD-lipid system.

MD simulations

The CHARMM36 force field was used to describe the protein, the lipid bilayer, and the ions (Klauda et al., 2010). CBD was parameterized using the SwissParam software (Zoete et al., 2011). The TIP3P water model was used to describe the water molecules. The systems were minimized for 5,000 steps using steepest descent and equilibrated with a constant number of particles, pressure, and temperature for at least 450 ps for the lipid-CBD system and 36 ns for the Nav1.4-CBD-lipid system, during which the position restraints were gradually released according to the default CHARMM-GUI protocol. During equilibration and production, a time step of 2 fs was used; pressure was maintained at 1 bar through Berendsen pressure coupling; temperature was maintained at 300°K through Berendsen temperature coupling with the protein, membrane, and solvent coupled; and the linear constraint solver algorithm (Hess et al., 1997) was used to constrain the bonds containing hydrogen. For long-range interactions, periodic boundary conditions and particle mesh Ewald were used. For short-range interactions, a cutoff of 12 Å was used. Finally, unrestrained production simulations were run for 150 ns for each of the lipid-CBD systems and for 10 ns for the Nav1.4-CBD-lipid system, using Parrinello-Rahman pressure coupling (Parrinello and Rahman, 1981) and Nosé-Hoover temperature coupling (Nosé, 1984). Simulations were performed using GROMACS 2018.4 (Abraham et al., 2015).

Adiabatic bias MD (ABMD) simulations

ABMD (Marchi and Ballone, 1999) simulations were performed using GROMACS 2018.4 (Abraham et al., 2015) patched with PLUMED 2.5.1 (Tribello et al., 2014) to study the entrance

pathway of CBD into its docking site in hNav1.4. ABMD is a simulation method in which a time-dependent biasing harmonic potential is applied to drive the system toward a target system along a predefined collective variable. Whenever the system moves closer toward the target system along the collective variable, the harmonic potential is moved to this new position, resulting in pushing the system toward the final state. The bias potential was applied along the distance between the center of masses of CBD and F1586. Two types of biasing potentials were considered: one along the y component of distance and the other along all components of distance.

²H NMR lipid analysis

POPC-d31, sn-1 chain perdeuterated, was obtained from Avanti Polar Lipids. The POPC-d31:CBD sample was prepared with ~50 mg lipid and 3.4 mg CBD for a POPC/CBD ratio of 8:2. The two samples, pure POPC-d31 and POPC-d31:CBD (8:2), were dissolved in Bz/MeOH 4:1 (vol/vol) and freeze dried. After hydration with excess amounts of deuterium-depleted water, five freeze-thaw-vortex cycles were used between liquid nitrogen (-196°C) and 60°C to create multilamellar dispersions.

Deuterium ²H NMR experiments were performed on a Tac-Mag Scout spectrometer at 46.8 MHz using the quadrupolar echo technique. The spectra were produced from ~20,000 two-pulse sequences. 90° pulse lengths were set to 3.1 μs, interpulse spacing was 50 μs, dwell time was 2 μs, and acquisition delays were 300 ms. Data were collected using quadrature with Cyclops eight-cycle phase cycling. The spectra were dePaked to extract the smoothed order parameter profiles of the POPC sn-1 chain in the presence or absence of CBD. Samples were run at 20°C, 30°C, and 40°C, and then left to equilibrate at each temperature for 20 min before measurements were taken.

Gramicidin-based fluorescence membrane elasticity assay (GFA)

1,2-Dierucoyl-sn-glycero-3-phosphocholine (DC_{22:1}PC) was from Avanti Polar Lipids. CBD was from Sigma-Aldrich. 8-Aminonaphthalene-1,3,6-trisulfonate (ANTS) was from Invitrogen/Life Technologies. Gramicidin D was from Sigma-Aldrich.

For the GFA, large unilamellar vesicles (LUVs) were made from DC_{22:1}PC as described previously (Rusinova et al., 2015). Briefly, phospholipids in chloroform and gramicidin A (gA) in methanol (1,000:1 lipid:gA weight ratio) were mixed. Quench rates were obtained by fitting the quench time course from each mixing reaction with a stretched exponential (Ingólfsson et al., 2010):

$$F(t) = F(\infty) + (F(0) - F(\infty)) \cdot \exp\left[-(t/\tau_0)^\beta\right] \quad (1)$$

and evaluating the quench rate at 2 ms (the instrumental dead time is ~1.5 ms):

$$k(t) = (\beta/\tau_0) \cdot (t/\tau_0)^{(\beta-1)} \Big|_{2\text{ms}} \quad (2)$$

To test drug effects on the lipid bilayer, CBD was equilibrated with the LUVs for 10 min at 25°C before acquiring quench time courses. Each measurement consisted of four to eight individual

mixing reactions, and the rates for each mixing reaction were averaged and normalized to the control rate in the absence of drug.

Compound preparation

CBD, lidocaine, or flecainide powder dissolved in 100% DMSO was used to prepare extracellular solutions at different concentrations with no more than 0.5% total DMSO content. Dilutions were performed in buffered solutions. The compound concentrations used in patch-clamp experiments were based on information obtained from the literature (Ghovanloo et al., 2018c). We previously determined that the resting-state half-maximal inhibitory concentration (IC_{50}) of CBD in Nav is ~ 10 μ M, with 1–2 μ M CBD being high enough to impart detectable changes in Nav gating but not blocking too much of the peak current amplitude. 40 mM CBD and 100 mM lidocaine were used in the isothermal titration calorimetry (ITC) experiment, as it is typical to use high compound concentrations in these experiments to detect heat changes. Saturating levels of CBD (100 μ M) and tetrodotoxin (TTX; 300 nM) were used in myography experiments to survey possible reductions in muscle contractility.

Cell culture

CHOK1 Chinese hamster ovary cells were transiently cotransfected with cDNA encoding enhanced GFP and the $\beta 1$ -subunit and either WT-Nav1.4 (GenBank accession no. NM_000334) or any of our mutant α -subunits. Transfection was done according to the PolyFect transfection protocol. After each set of transfections, a minimum of 8 h of incubation was allowed before plating on sterile coverslips. All cells were incubated at 37°C/5% CO₂.

Patch-clamp recordings

Whole-cell patch-clamp recordings were performed in an extracellular solution containing (in mM) 140 NaCl, 4 KCl, 2 CaCl₂, 1 MgCl₂, and 10 HEPES or Mes (pH 6.4). Solutions were adjusted to pH 6.4 and 7.4 with CsOH. Pipettes were filled with intracellular solution containing (in mM) 120 CsF, 20 CsCl, 10 NaCl, and 10 HEPES. In some experiments, lower sodium concentration of 1 mM (intracellular) was used to boost driving force, hence current size. All recordings were made using an EPC-9 patch-clamp amplifier (HEKA Elektronik) digitized at 20 kHz via an ITC-16 interface (Instrutech). Voltage clamping and data acquisition were controlled using PatchMaster/FitMaster software (HEKA Elektronik) running on an Apple iMac. Current was low-pass filtered at 10 kHz. Leak subtraction was performed automatically by software using a P/4 procedure following the test pulse. Gigaohm seals were allowed to stabilize in the on-cell configuration for 1 min before establishing the whole-cell configuration. Series resistance was < 5 M Ω for all recordings. Series resistance compensation up to 80% was used when necessary. All data were acquired at least 1 min after attaining the whole-cell configuration. Before each protocol, the membrane potential was hyperpolarized to -130 mV to ensure complete removal of both fast inactivation and slow inactivation. All experiments were conducted at $22 \pm 2^\circ$ C. Analysis and graphing were done using FitMaster software (HEKA Elektronik) and Igor Pro

(Wavemetrics). All data acquisition and analysis programs were run on an Apple iMac.

Some cDNA constructs produced small ionic currents. To ensure the recorded currents were indeed construct-produced currents and not endogenous background currents, untransfected cells were patched and compared with transfected cells. The untransfected CHOK1 cells, which were exclusively used for cDNA expression, produced no endogenous sodium currents. Compound effects were measured after currents were stable (see Fig. S5).

Activation protocol

To determine the voltage dependence of activation, we measured the peak current amplitude at test pulse potentials ranging from -100 mV to $+80$ mV in increments of $+10$ mV for 20 ms. Channel conductance (G) was calculated from peak I_{Na} :

$$G_{Na} = I_{Na} / V - E_{Na}, \quad (3)$$

where G_{Na} is conductance, I_{Na} is peak sodium current in response to the command potential V , and E_{Na} is the Nernst equilibrium potential. Calculated values for conductance were fit with the Boltzmann equation:

$$G / G_{max} = 1 / \{1 + \exp[-ze_0(V_m - V_{1/2})] / kT\}, \quad (4)$$

where G/G_{max} is normalized conductance amplitude, V_m is the command potential, z is the apparent valence, e_0 is the elementary charge, $V_{1/2}$ is the midpoint voltage, k is the Boltzmann constant, and T is temperature in K.

Steady-state fast inactivation (SSFI) protocol

The voltage dependence of fast inactivation was measured by preconditioning the channels to a hyperpolarizing potential of -130 mV (for 200 ms) and then eliciting prepulse potentials that ranged from -170 to $+10$ mV in increments of 10 mV for 200/800 ms, followed by a 10-ms test pulse during which the voltage was stepped to 0 mV. Normalized current amplitudes from the test pulse were fit as a function of voltage using the Boltzmann equation:

$$I / I_{max} = 1 / \{1 + \exp[-ze_0(V_m - V_{1/2})] / kT\}. \quad (5)$$

where I_{max} is the maximum test pulse current amplitude.

Persistent current protocol

Persistent current was measured between 145 and 150 ms during a 200-ms depolarizing pulse to 0 mV from a holding potential of -130 mV. Pulses were averaged to increase signal-to-noise ratio.

Recovery from fast inactivation protocol

Channels were fast inactivated during a 500-ms depolarizing step to 0 mV, and recovery was measured during a 19-ms test pulse to 0 mV following a -130 -mV recovery pulse for durations between 0 and 4 s. This protocol has been used extensively to measure recovery from fast inactivation (Featherstone et al., 1996; Richmond et al., 1998; Sokolov et al., 2013; Hampl et al., 2016; Ghovanloo et al., 2020). Time constants of fast inactivation recovery showed two components and were fit using a double exponential equation:

$$I = I_{ss} = \alpha_1 \exp(-t/\tau_1) + \alpha_2 \exp(-t/\tau_2), \quad (6)$$

where I is current amplitude, I_{ss} is the plateau amplitude, α_1 and α_2 are the amplitudes at time 0 for time constants τ_1 and τ_2 , and t is time.

ITC

The peptide with the sequence SYIIISFLIVVNM (from Nav1.4 domain IV [DIV]-S6, residues 1580–1592) was synthesized by GenScript. It was solubilized in DMSO and diluted to a final concentration of 1 mM with the final buffer containing, by percentage, 10% DMSO, 60% acetonitrile, and 30% ITC buffer. Acetonitrile was required to solubilize the peptide. The ITC buffer contained 50 mM HEPES, pH 7.2, and 150 mM KCl. CBD and lidocaine were each solubilized in DMSO and diluted to final concentrations of 40 mM and 100 mM, respectively, in the same final buffer as the peptide. Each titrant was injected into the peptide containing sample cells 13 times each with a volume of 3 μ M, with the exception of the first injection, which was 0.4 μ M. Stirring speed was set at 750 rpm.

AP modeling

Skeletal AP modeling was based on a model developed by Cannon et al. (1993). All APs were programmed and run using Python. The modified parameters were based on electrophysiological results obtained from whole-cell patch-clamp experiments (Cannon et al., 1993). The model accounted for activation voltage dependence, SSFI voltage dependence, and persistent I_{Na} (Table S3). The WT pH 7.4 model uses the original parameters from the model. P1158S models were programmed by shifting parameters from the original Cannon model by the difference between the values in P1158S experiments at a given pH/CBD (Ghovanloo et al., 2018a; Cannon et al., 1993).

Statistics

A t test was used to compare the mean responses. All statistical P values report the results obtained from tests that compared experimental conditions with the control conditions. A level of significance of $\alpha = 0.05$ was used with P values < 0.05 being considered to be statistically significant. All values are reported as mean \pm SEM for n recordings/samples. Power analysis with $\alpha = 0.05$ was performed to yield sufficient n size for each experiment. Analysis was performed in JMP version 14.

Online supplemental material

Fig. S1 shows Nav1.4 WT interactions with CBD. Fig. S2 shows sample normalized time dependence. Fig. S3 shows ^2H NMR at different temperatures and further characterization of F1586A. Fig. S4 shows Nav1.4 F1586A interactions with CBD. Fig. S5 shows further characterization of F1586A. Fig. S6 shows CBD interactions with DIV-S6, using ITC. Fig. S7 shows a structural integrity MD simulation of the CBD pathway through the Nav1.4 fenestration. Fig. S8 shows CBD concentration dependence and varying pulse duration fast inactivation (F-I) curve measurement. Fig. S9 shows WWWW characterization. Fig. S10 shows a comparison between some of the relevant physicochemical properties of the compounds used in this study. Video 1 depicts

CBD localization inside a POPC membrane. Video 2 is an ABMD simulation which shows that CBD passes through the fenestration of Nav1.4 (bias applied along y component of distance). Video 3 is an ABMD simulation which shows that CBD passes through the fenestration of Nav1.4 (bias applied along all components of distance). Table S1 shows data comparing CBD inhibition of Nav1.4 at two different frequencies. Table S2 shows the numbers associated with MD simulation systems. Table S3 shows the numbers associated with AP modeling.

Results

MD simulations predict CBD accumulates in the hydrophobic region of phospholipid bilayers

We previously determined that CBD nonselectively inhibits voltage-dependent sodium and potassium currents with a steep average Hill slope of ~ 3 , which suggested multiple interactions. Contrary to what is expected for classic pseudo-second-order bimolecular blocking schemes, we found CBD was fastest to equilibrate and most potent at lower temperatures (Ghovanloo et al., 2018c). These findings, together with CBD's stabilizing effects on neuronal Nav inactivation and CBD's high partition coefficient (LogP) of ~ 5.9 , led us to explore whether CBD alters membrane elasticity, which indirectly could inhibit Nav currents (Ghovanloo et al., 2018c), similar to what has been suggested for amphiphilic compounds (Lundbæk et al., 2004, 2005). To test this hypothesis, we performed MD simulations of CBD (with a ratio of 2, 3, or 6 to 188 CBD:POPC molecules, respectively) on POPC lipid membranes for hundreds of nanoseconds (Fig. 1, a–e; Table S1). The MD results indicate that in both symmetrical (i.e., the same number of CBD molecules in both leaflets of the membrane) and asymmetrical (i.e., CBD in a single leaflet) conditions, there are no substantial changes in the area per lipid (Fig. 1 a). Indeed, a small shift in the peak of the distribution can only be seen for system 3: while the peak for systems 0, 1, and 2 is $\sim 0.63 \text{ nm}^{-2}$, it is $\sim 0.645 \text{ nm}^{-2}$.

Fig. 1 c shows CBD density estimates as a function of the membrane leaflet coordinate, where the lipid bilayer is centered at 0 (membrane thickness, measured as the average distance between the phosphorus atom in the opposite leaflet, remains unchanged across conditions). In symmetrical conditions, there are two density peaks in both negative and positive coordinate ranges with an almost perfect overlap and CBD is localized to the region between the lipid headgroups and the membrane center, close to the lipid headgroup region. In the asymmetric condition, with three CBD molecules initially placed in the leaflet to the right, there is only a single peak in the positive coordinate range. The MD results show that CBD molecules tend to reside in the leaflet to which they originally were added, where they interact with, and detach rapidly from, polar residues at the bilayer-resolution interface and occasionally move toward the aqueous phase outside the membrane, then move back into the membrane's hydrophobic core (Video 1). This suggests that, within the time frame of hundreds of nanoseconds in our simulations, CBD does not diffuse across the two leaflets but instead tends to localize in the leaflet where it was initially placed. While we cannot rule out the possibility that CBD diffuses across the two

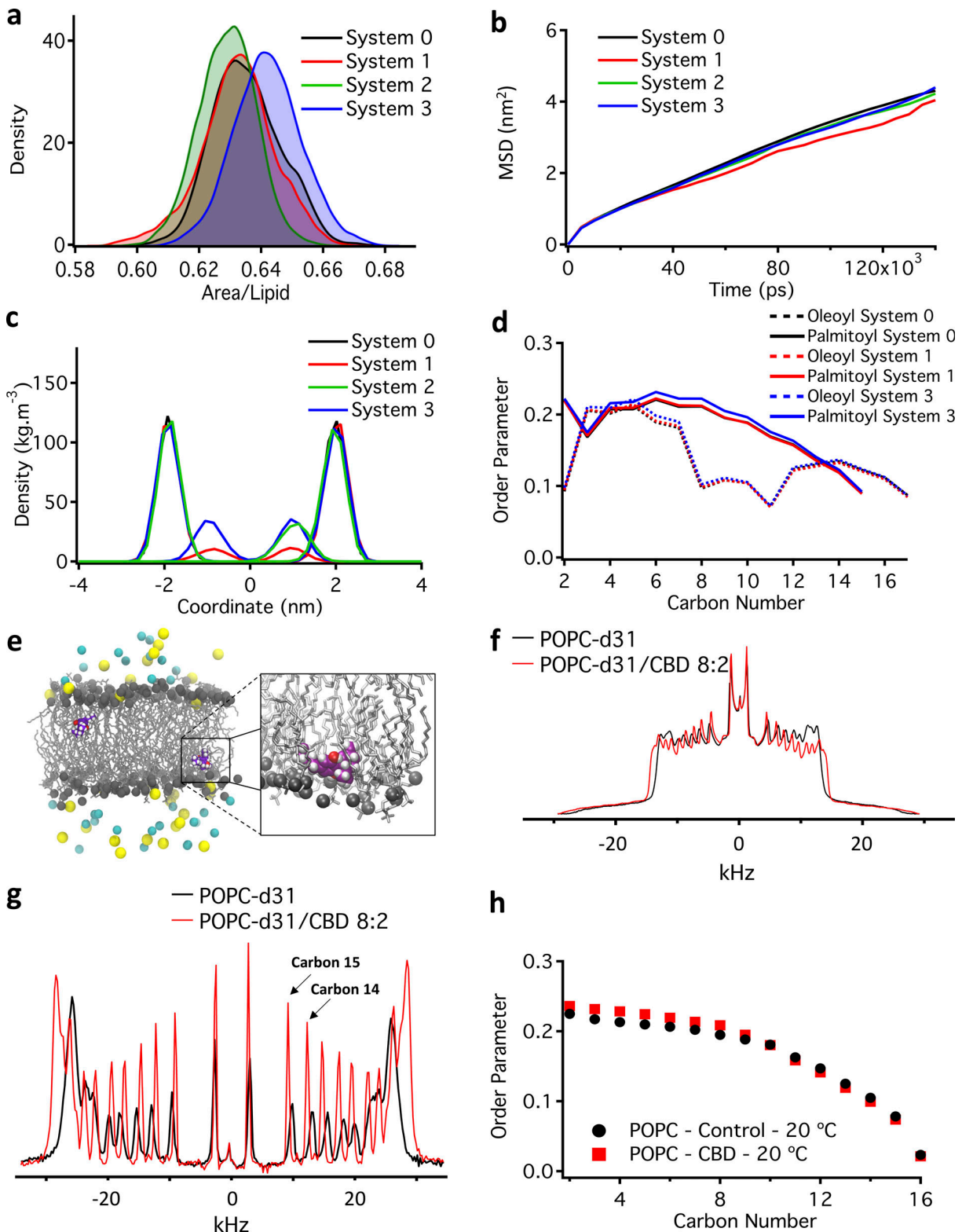


Figure 1. Effects of CBD on POPC membrane via MD simulations and ²H NMR. (a and b) The effects of CBD on POPC membrane area per lipid and lipid diffusion. System 0 is the control; system 1 is two CBD molecules in symmetry (one in each leaflet); system 2 is three CBD molecules in asymmetry (only in a single leaflet); and system 3 is six CBD molecules in symmetry (three in each leaflet). Area per lipid (a) and mean square displacement as a function of time (b) are not affected by CBD. (c) Distribution of CBD into the membrane across a range of conditions. The distribution of phosphate groups is shown as solid lines and the distribution of CBD is shown as dotted lines. The bilayer thickness remains ~4 nm in the presence and absence of CBD. (d) Order parameter of lipid acyl chains estimated from the MD simulations. (e) Snapshot of a CBD molecule in the POPC leaflet extracted from the MD simulations (see Video 1). The zoomed-in image shows localization of CBD molecule below the leaflet headgroup. (f) NMR spectra collected at 20°C. (g) The spectra in f have been dePacked, showing doublets that correspond to individual palmitoyl methylene and methyl groups. The frequency separation of a given doublet is directly proportional to its order parameter. (h) The effect of CBD on the NMR order parameter profile of POPC-d31's palmitoyl chain.

leaflets over longer timescales, the effect we observed is compatible with a substantial free energy barrier related to membrane permeation. The preferred localization seems to come from the combination of oxygen atoms keeping CBD from diffusing across leaflets and from CBD's hydrophobic tail keeping it from getting too close to water molecules outside the membrane.

²H NMR verifies the MD predictions regarding localization

Overall, the MD results suggest that CBD preferentially localizes under the phosphate heads, close to carbons 3–7 of the aliphatic chains of the POPC molecules (Fig. 1 e). Next, we estimated acyl chain order parameters from the MD simulation data. CBD appeared to cause a slight ordering of the membrane methylenes in the plateau region of the palmitoyl chain (shown as an increase in order parameter for C3–C8) and in the C3–C7 region of the oleoyl chain (Fig. 1 d).

We tested MD predictions regarding CBD localization using NMR (Lafleur et al., 1989) with multilamellar vesicles POPC-d31 and POPC-d31/CBD at a 4:1 ratio in deuterium-depleted water at three different temperatures (20°C, 30°C, and 40°C; Fig. 1, f–h; and Fig. S1 a–c). Calculating order parameters from NMR provides indeed a direct connection with the MD simulations and, if in agreement, would confirm the predictive power of the MD simulations with respect to CBD localization. Indeed, the NMR results were in striking agreement with the MD predictions of the changes in acyl chain order parameters and showed that CBD causes an ordering of the C2–C8 palmitoyl chain methylenes and a slight disordering from C10 to C15 in a temperature-dependent manner. This unusual biphasic effect of CBD on membrane chain organization suggests that CBD molecules insert into the hydrophobic region of the membrane and tend to localize near the lipid–water interface, ordering nearby acyl chain methylenes and allowing reduced packing density and increased fluidity of the ends of the acyl chains. Thus, the NMR results are in striking agreement with the MD predictions of the preferred intramembrane location of CBD.

CBD alters bilayer elasticity in GFA

The MD and NMR results show that CBD increases the order parameter of the bilayer core, which would tend to make bilayers thicker and less elastic. We tested this prediction using the bilayer-spanning gramicidin channels, which form by transmembrane dimerization of two nonconducting monomers (O'Connell et al., 1990). The conducting channel's hydrophobic length is less than the host bilayer's hydrophobic thickness (e.g., Lundbæk et al., 2010; see also Fig. 2 a), meaning that channel formation is associated with a local bilayer deformation/thinning, which has an associated energetic cost, the bilayer deformation energy (ΔG_{def}), and the difference between the deformation energies associated with the nonconducting monomers ($\Delta G_{\text{def}}^{\text{M}}$) and conducting dimers ($\Delta G_{\text{def}}^{\text{D}}$), and the bilayer contribution to the gramicidin monomer↔dimer equilibrium will be $\Delta G_{\text{bilayer}}^{\text{M} \rightarrow \text{D}} = \Delta G_{\text{def}}^{\text{D}} - \Delta G_{\text{def}}^{\text{M}}$. The magnitude of ΔG_{def} depends on the channel–bilayer hydrophobic mismatch and the bilayer elastic properties; for a given deformation, $\Delta G_{\text{def}}^{\text{D}}$ will increase as the bilayer elasticity decreases (the stiffness increases). Based on the MD and NMR results, we thus

would predict that CBD would inhibit the formation of conducting channels (shift the monomer↔dimer equilibrium toward the nonconducting monomers).

We tested CBD's effects on lipid bilayer properties at concentrations where CBD has acute effects on Nav channels using a GFA, which takes advantage of the gramicidin channels' unique sensitivity to changes in bilayer properties (Andersen and Koeppel, 2007). The GFA is based on the gramicidin channels' permeability to Tl⁺, a quencher of the water-soluble fluorophore ANTS, which can be encapsulated in LUVs that have been doped with gramicidin. The rate of Tl⁺ influx, the rate of fluorescence quench, is a measure of the time-averaged number of gramicidin channels in the LUV membrane (Ingólfsson et al., 2010). As noted above, molecules that alter the thickness and elasticity of the LUV membrane will alter the lipid bilayer contribution to the free energy of dimerization:

$$\frac{[\text{D}]}{[\text{M}]^2} = K^{\text{M} \rightarrow \text{D}} = \exp \left\{ \frac{\Delta G_{\text{protein}}^{\text{M} \rightarrow \text{D}} + \Delta G_{\text{bilayer}}^{\text{M} \rightarrow \text{D}}}{k_{\text{B}} T} \right\},$$

which will produce a shift in the gramicidin monomer↔dimer equilibrium (Fig. 2 a) and thereby change the average number of conducting dimers in the LUV membrane, which we can measure as changes in the rate of Tl⁺ influx (rate of fluorescence quench). As would be expected from the MD and NMR results, CBD reduced the Tl⁺ influx rates in a concentration-dependent manner (structures in Fig. 2, b–e). For comparison, we also show in Fig. 2 e the results we obtained with Triton X-100 from Ingólfsson et al. (2010), which increased the quench rates demonstrating that these two molecules have opposite effects on the membrane, and we conclude that CBD indeed increases bilayer stiffness or thickness, whereas Triton X-100 decreases bilayer stiffness or thickness. Given that CBD has minimal effects in bilayer thickness (Fig. 1), we conclude that CBD decreases lipid bilayer elasticity.

CBD interacts with the Nav LA site

We previously found that CBD displays an ~10-fold state dependence (10-fold increased affinity for inactivated state) in Nav inhibition, a property similar to classic pore blockers (Ghovanloo et al., 2018c; Kuo and Bean, 1994; Bean et al., 1983), which has also been observed with bilayer-modifying molecules (Lundbæk et al., 2005). In our previous study, we tested CBD inhibition from the inactivated state in a Nav1.1 pore mutant (F1763A–LA mutant; Ghovanloo et al., 2018c), and the results suggested an ~2.5-fold decrease in potency (Ghovanloo et al., 2018c). To further explore possible CBD interactions at the pore, we performed molecular docking using the human Nav1.4 cryo-EM structure (Pan et al., 2018). While molecular docking is a fast-search method that can only approximate docking sites, it is useful to narrow down the number of mutagenesis experiments to perform. Fig. 3, a and b, shows CBD docked onto the Nav1.4 pore in its most favorable binding pose, supporting a possible interaction at the LA site. Another docking site predicted to be of slightly lower binding affinity is found at another fenestration, at a site of similar geometry to the LA site (Fig. S2, a–d).

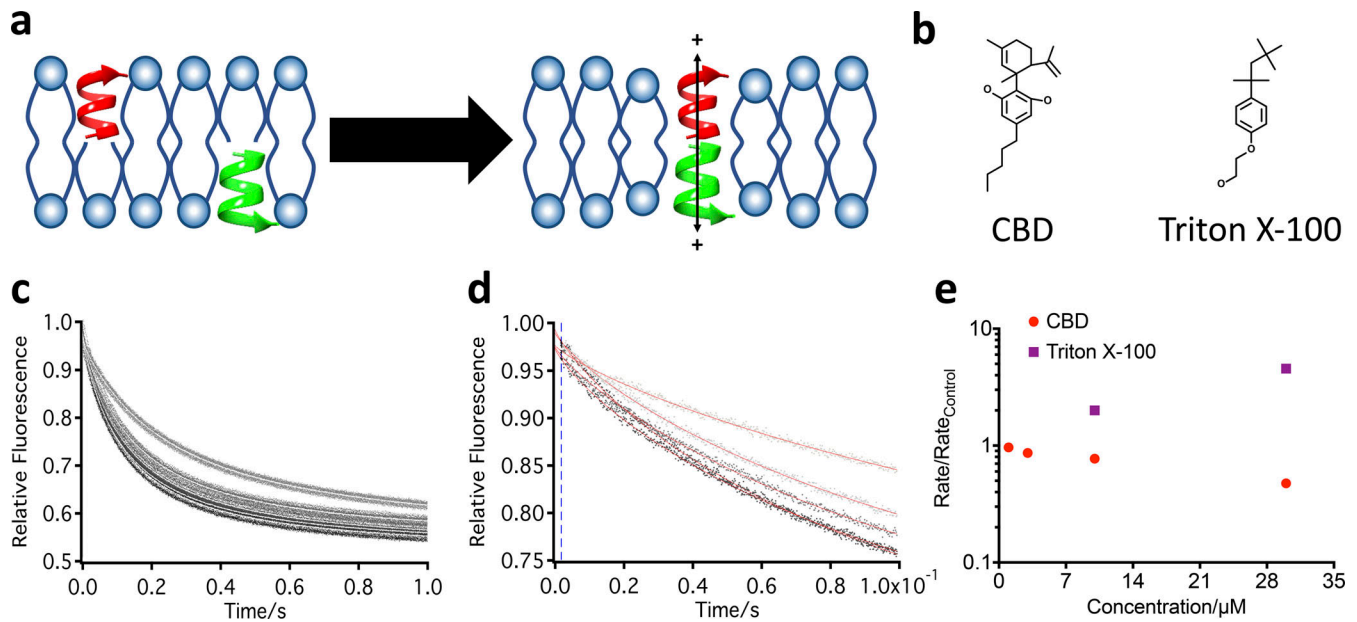


Figure 2. CBD alters lipid bilayer properties in GFA. **(a)** Cartoon representation of gramicidin monomers in each leaflet coming together (dimerizing) to form cationic channels. The dimerization of the gramicidin channels is directly related to membrane elasticity. These properties are used to assay compound (e.g., CBD) effects on membrane elasticity. **(b)** Chemical structures of CBD and Triton X-100. **(c)** Fluorescence quench traces showing Tl⁺ quench of ANTS fluorescence in gramicidin-containing DC_{22:1}PC LUVs with no drug (control, black) and incubated with CBD for 10 min at the noted concentrations. The results for each drug represent five to eight repeats (dots) and their averages (solid white lines). **(d)** Single repeats (dots) with stretched exponential fits (red solid lines). **(e)** Fluorescence quench rates determined from the stretched exponential fits at varying concentrations of CBD (red) and Triton X-100 (purple, from Ingólfsson et al., 2010) normalized to quench rates in the absence of drug. Mean ± SD, n = 2 (for CBD).

We also docked CBD onto F1586A, which suggested that having an alanine at position 1586 (instead of the WT phenylalanine) destabilizes the CBD interaction at the Nav1.4 pore (Fig. S3, a–d). Fig. 3, c–f, shows biophysical characterization of F1586A compared with WT-Nav1.4. Both channels have similar properties, and, most importantly, the inactivation voltage dependences were almost identical ($P > 0.05$); however, F1586A had a faster τ_{slow} than WT-Nav1.4 ($P < 0.05$; Fig. 3 f; for further characterization, see Fig. S4), suggesting that at any given potential, both F1586A and Nav1.4 would have the same availability. Therefore, resting-state pharmacological experiments could be performed from the same holding potential on both channels (i.e., both channels are fully available from a -110 -mV holding potential, which is what was used in subsequent experiments; Fig. 3 f).

In contrast to neuronal Navs that have inactivation midpoints ($V_{1/2}$) of approximately -65 mV in some neurons with resting membrane potentials (RMPs) that are, on average, approximately -75 to -65 mV (Buchanan, 1993; Williams et al., 2002), Nav1.4 has a $V_{1/2}$ of approximately -65 mV in skeletal muscle fibers with an RMP of approximately -90 mV (Cannon et al., 1993). This indicates that, whereas neuronal Navs are half-inactivated at RMP, Nav1.4 is almost fully available at RMP. Therefore, we measured lidocaine (positive control) and CBD inhibition of Nav1.4 from rest (-110 -mV holding potential to 0 mV, test pulse at 1 Hz) to be closer to physiological conditions (Fig. 3, g and h). Our results show that 1.1 mM (resting IC_{50} on Nav1.4; Nuss et al., 1995) lidocaine blocks $\sim 60\%$ of I_{Na} in WT and $\sim 20\%$ in F1586A ($P = 0.020$). 10 μM CBD blocks $\sim 45\%$ I_{Na} in WT

and $\sim 25\%$ in F1586A ($P = 0.037$). Hence, there is a threefold difference between lidocaine's inhibition of WT versus F1586A and a smaller 1.5-fold difference for CBD inhibition. This suggests that, whereas CBD may interact with the Nav pore similar to lidocaine, CBD's interaction with F1586 may not be a critical determinant of its I_{Na} inhibition (as compared with lidocaine). This is supported by the difference in interaction site between CBD and PII (analgesic compound) shown in NavMs (sodium channel from *Magnetococcus marinus*) using crystallography (Sait et al., 2020). Another possible underlying reason for the weaker CBD inhibition of F1586A could be due to construct-dependent reduced occupancy of slow inactivated states, as F1586A has a faster τ_{slow} than WT-Nav1.4 in its recovery from a 500-ms prepulse (Fig. S4). However, because the results shown in Fig. 3, g and h, were taken by holding at -110 mV and pulsed at 1 Hz (giving enough time to reset channels to resting state), it seems less likely that slow inactivation causes the weaker inhibition of F1586A. To ensure there is no test pulse-mediated confounding effect, we compared CBD block of Nav1.4 at 0.2 and 1 Hz, which showed no statistically significant difference ($P > 0.05$; Table S1).

We previously measured the kinetics of CBD block of Nav1.2 at three different temperatures and found that, while relatively slow at all temperatures, blocking is fastest at lower temperatures. At $\sim 20^\circ\text{C}$ (the approximate temperature at which our recordings were performed in this study), CBD reaches equilibrium within ~ 400 s (Ghovanloo et al., 2018c). Therefore, in this study, our Nav1.4 patch-clamp measurements were performed after ~ 400 -s incubation with CBD. Sample normalized time dependence recordings for resting-state block of CBD,

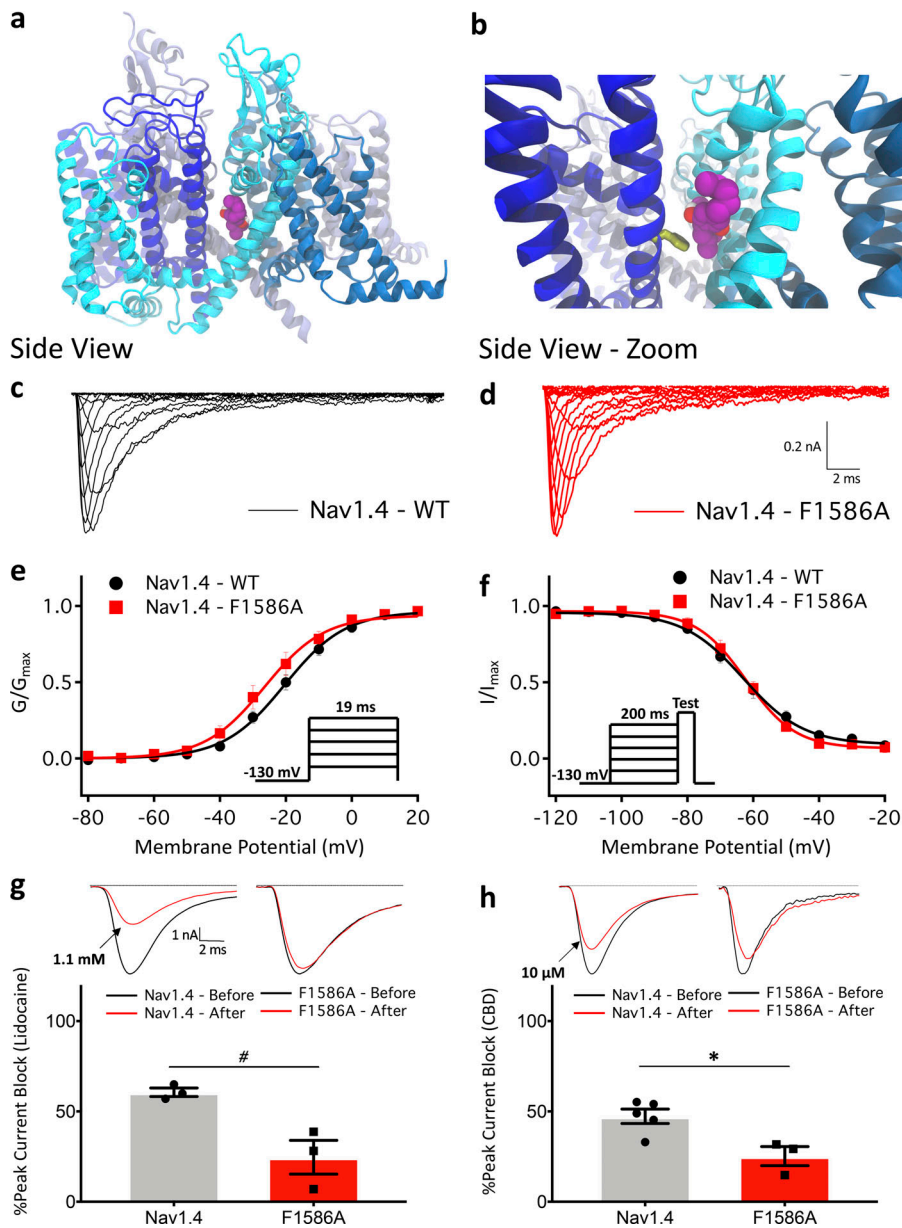


Figure 3. Inhibition of Nav1.4 pore by CBD, F1586A reduces inhibition. (a) Side view of CBD docked into the pore of the human Nav1.4 structure. The structure is colored by domain. DIV is colored in deep blue. (b) Zoomed-in side view in which F1586 is colored yellow. (c and d) Representative families of macroscopic current traces from WT-Nav1.4 and F1586A. (e) Voltage dependence of activation as normalized conductance plotted against membrane potential (Nav1.4: $V_{1/2} = -19.9 \pm 2.7$ mV, $z = 2.8 \pm 0.3$, $n = 5$; F1586A: $V_{1/2} = -22.4 \pm 2.2$ mV, $z = 3.0 \pm 0.3$, $n = 7$; $P > 0.05$ for both $V_{1/2}$ and z). (f) Voltage dependence of SSFI as normalized current plotted against membrane potential. Channels were held at -130 mV for 200 ms (Nav1.4: $V_{1/2} = -64.1 \pm 2.4$ mV, $z = -2.7 \pm 0.3$, $n = 8$; F1586A: $V_{1/2} = -63.3 \pm 3.0$ mV, $z = -3.5 \pm 0.3$, $n = 8$; $P > 0.05$ for both $V_{1/2}$ and z). (g and h) Lidocaine/CBD inhibition of Nav1.4 and F1586A from -110 mV (rest) at 1 Hz with a 20-ms depolarizing pulse (lidocaine-Nav1.4: mean block = $60.6 \pm 2.3\%$, $n = 3$, $\#$, $P = 0.020$; CBD-Nav1.4: mean block = $47.3 \pm 3.7\%$, $n = 5$; CBD-F1586A: mean block = $25.3 \pm 4.8\%$, $n = 3$, $*$, $P = 0.037$). Sample traces before and after compound perfusion are shown. All values in e–h are reported as mean \pm SEM.

lidocaine, flecainide, and a negative control (no compound to ensure the slow CBD effect is not due to run-down) are shown in Fig. S5.

CBD interacts with DIV-S6

Because CBD's I_{Na} inhibition was less affected by F1586A, a mutation that destabilizes the LA binding site, than a well-established pore blocker such as lidocaine, we investigated whether CBD interacts with the DIV-S6 (which includes F1586) or if it is inert, using ITC. We then compared CBD interactions to lidocaine. We found that both lidocaine and CBD appear to interact with the protein segment, though the nature of this interaction seems to differ (Fig. S6). Fig. S6, a and b, shows sample ITC heat traces. Our results suggested that, in the presence of protein, lidocaine titration causes an endothermic interaction. However, when the protein is absent, lidocaine titration into blank buffer causes exothermicity. In contrast, CBD titration

both in blank buffer and in the presence of protein resulted in endothermic responses, with the magnitude of CBD's heats of interaction being approximately fourfold larger in the protein condition than in the blank condition. This was in contrast to lidocaine that showed comparable heats of interaction magnitudes in both conditions, but in different directions. To quantify interactions of both lidocaine and CBD, we subtracted the heats from runs with both protein and ligand subtracted from only ligand (blank). The subtracted heats show a similar trend between lidocaine and CBD (Fig. S6, c and d). These results suggest that both lidocaine and CBD interact with the protein segment; however, the nature of this interaction is different, possibly due to a variation in physicochemical properties.

CBD may penetrate into the pore through fenestrations

LAs block bacterial Navs in their resting state by entering the pore through fenestrations in a size-dependent manner

(i.e., smaller LAs get through more readily; Gamal El-Din et al., 2018). Here, we sought to determine whether it is possible to block CBD's access to the human Nav1.4 pore from the lipid phase of the membrane by occluding fenestrations. We previously found that CBD is highly lipid bound (99.6%; Ghovanloo et al., 2018c), and our MD results show that it preferentially localized in the hydrophobic part of the membrane, just below the lipid headgroups. Therefore, we reasoned that once CBD partitions into the membrane, it will have access to the Nav pore through the intramembrane fenestrations. To test this idea, we scrutinized the docking pose of CBD in the human Nav1.4 and observed its localization close to the fenestrations (Fig. 4 a). The CBD docking pose inside the Nav1.4 fenestrations is in close agreement with recent findings using x-ray crystallography to show the binding of CBD inside the bacterial NavMs (Sait et al., 2020).

Next, we identified four residues (DI-F432, DII-V787, DIII-I1280, and DIV-I1583) that partially or fully occluded the fenestrations when mutated to tryptophan (W), as predicted by computational mutagenesis and structural minimization (the predicted partial versus full occlusion is due to structural asymmetry of mammalian Navs; Fig. 4, b and c). However, as Nav channels are dynamic proteins, both of the computationally predicted fenestration occlusion poses are likely to be partial in nature; therefore, we refer to the occlusion construct (WWWW) as a fenestration-altered construct with two mutational poses: pose 1 (computationally fully occluded) and pose 2 (computationally partially occluded).

We measured resting-state block of 1.1 mM lidocaine, 350 μ M flecainide, and 10 μ M CBD from -110 mV on our WWWW construct. Our results suggest that lidocaine ($P > 0.05$) and flecainide ($P > 0.05$), but not CBD ($P < 0.05$), blocked the WWWW mutant the same as WT (after compound has reached equilibrium; Figs. 4 d and S2). This is an interesting result considering that CBD is larger than lidocaine but slightly smaller than flecainide. CBD was inert with respect to block of WWWW, relative to WT-Nav1.4, which suggests that CBD interacts with Nav1.4 via the fenestrations.

To visualize the possible pathway CBD follows through Nav1.4 fenestrations and into the pore at an atomistic resolution, we performed MD simulations in which we encouraged CBD to detach from its binding site (see Materials and methods; Fig. 4, e-g; Fig. S7; and Videos 2 and 3). These results demonstrate that CBD can enter its binding site in the pore through the fenestration without major reorganization of the channel structure.

CBD does not affect Nav1.4 activation but stabilizes the inactivated state

We previously characterized the effects of CBD on Nav1.1 gating (Ghovanloo et al., 2018c). We found that CBD at $-IC_{50}$ reduced channel conductance and did not change the voltage dependence of activation, but it produced a hyperpolarizing shift in SSFI and slowed recovery from fast (300 ms) and slow (10 s) inactivation (Ghovanloo et al., 2018c). Together with CBD's inhibition of resurgent sodium currents (Patel et al., 2016; Ghovanloo et al., 2018c), these results suggested that CBD prevents the opening of Navs but that the channels which can open, activate with

unchanged voltage dependence, and are more likely to inactivate. The overall effect is a reduction in excitability (Ghovanloo et al., 2018c). Here, we hypothesized that CBD's nonselectivity in I_{Na} inhibition suggests nonselectivity (i.e., CBD imparts similar gating modulation across Nav subtypes) in modulating Nav gating. To test this idea, we assessed Nav1.4 activation in the presence and absence of 1 and 2 μ M CBD by measuring peak channel conductance at membrane potentials between -100 and +80 mV (Fig. 5 a; and Fig. S8, a and b). CBD did not significantly alter $V_{1/2}$ or apparent valence (z) of activation ($P > 0.05$). Normalized Nav1.4 currents as a function of membrane potential are shown in Fig. 5 b. These results indicate that, as with Nav1.1, CBD does not alter Nav1.4 activation.

Next, we examined the voltage dependence of SSFI using a standard 200-ms prepulse voltage protocol from 1 and 2 μ M. Normalized current amplitudes were plotted as a function of prepulse voltage (Fig. 5 c; and Fig. S8, a and b). These results mimicked our previous observations in Nav1.1 (Ghovanloo et al., 2018c) in that CBD left shifted the Nav1.4 inactivation curve ($P < 0.05$).

To measure recovery from inactivation, we held Nav1.4 at -130 mV to ensure that the channels were fully available, then pulsed the channels to 0 mV for 500 ms and allowed different time intervals at -130 mV to measure recovery as a function of time. As previously observed in Nav1.1, CBD slowed the Nav1.4 recovery from inactivation ($P < 0.05$), suggesting that it takes longer for CBD to come off the channels than the time it takes the channels to recover from inactivation (Fig. 5 d). The τ_{Slow} and fraction of the recovery fit with τ_{Slow} are plotted in Fig. 5 e, which shows that CBD increases the fraction of recovery that is slow and the time constant of the slow component of recovery from inactivation from 500 ms. This indicates that CBD slows the recovery from inactivation, supporting the idea that CBD stabilizes the inactivated states. These results are consistent with our previous findings in Nav1.6 from 300-ms and 10-s pulse durations (Ghovanloo et al., 2018c). Because CBD slows recovery from inactivation, we also measured the effect of 1 μ M CBD on the voltage dependence of inactivation from an 800-ms prepulse, which showed a hyperpolarization of the curve (Fig. S8, c and d).

Because the proportion of channels populating different states is controlled by the membrane potential, the state dependence of such compounds is often termed voltage dependence. Many traditional Nav blockers also display use dependence, which occurs when the compound apparent potency increases upon higher sodium channel firing frequency stimulations (Gamal El-Din et al., 2018; Starmer et al., 1984). This feature is thought to be vital to compound efficacy against hyperexcitability conditions, including seizures and myotonic disorders (Desaphy et al., 2004; Eijkelkamp et al., 2012). To determine the effects of CBD (2 μ M) on use-dependent current reduction, we measured current amplitudes pulsed at 80 Hz (myotonic firing rates could go up to 80 Hz; Heatwole et al., 2013) for 12.5 s. Our results suggest that CBD accelerates the Nav1.4 use-dependent inactivation (Fig. 5 f).

We previously investigated the CBD state dependence in Nav1.1 (Ghovanloo et al., 2018c). Here, to further verify those

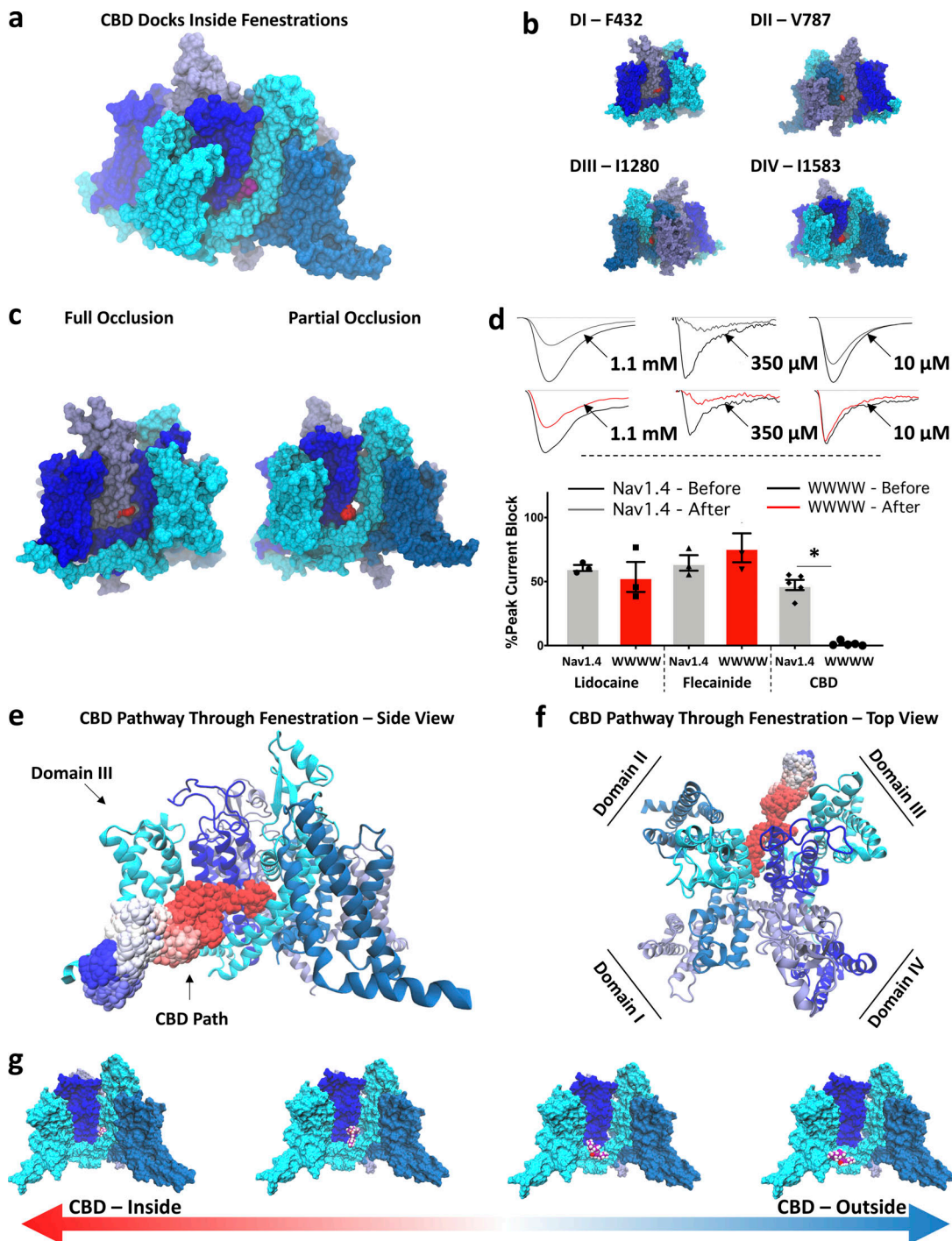


Figure 4. **CBD interactions with and through Nav fenestrations.** (a) Side view of CBD docked into the human Nav1.4 structure. The structure is colored by domain (matched color to domain is shown in f). CBD is represented in purple. (b) Side view of all four sides of human Nav1.4 (colored by domain). Nav1.4 fenestrations are highlighted in red, along with the position of respective residues that were mutated into tryptophans (W). (c) Computationally predicted mutagenesis of fenestrations results two full (pose 1) and two partial (pose 2) occlusions/alterations (paralleled domains). (d) Lidocaine (1.1 mM) inhibition of Nav1.4 and WWWW from -110 mV (rest) at 1 Hz 20 ms depolarizing pulse (Nav1.4: mean block = $60.6 \pm 2.3\%$, $n = 3$; WWWW: mean block = $53.6 \pm 11.7\%$, $n = 3$; $P > 0.05$), flecainide (350 μ M) inhibition (Nav1.4: mean block = $64.6 \pm 6.0\%$, $n = 3$; WWWW: mean block = $76.4 \pm 11.3\%$, $n = 3$; $P > 0.05$), and CBD (10 μ M) inhibition (Nav1.4: mean block = $47.3 \pm 3.7\%$, $n = 5$; WWWW: mean block = $6.4 \pm 1.3\%$, $n = 5$; *, $P = 0.0001$). Traces before and after compound perfusion are shown. Values are reported as mean \pm SEM. (e) CBD pathway through the Nav1.4 fenestration from side view, as predicted by MD simulations. Red and blue correlate with CBD being inside and outside the fenestration, respectively (see Videos 2 and 3). (f) CBD pathway from top view of the channel. (g) Progressive snapshots of the movement of CBD over time from inside to outside the channel.

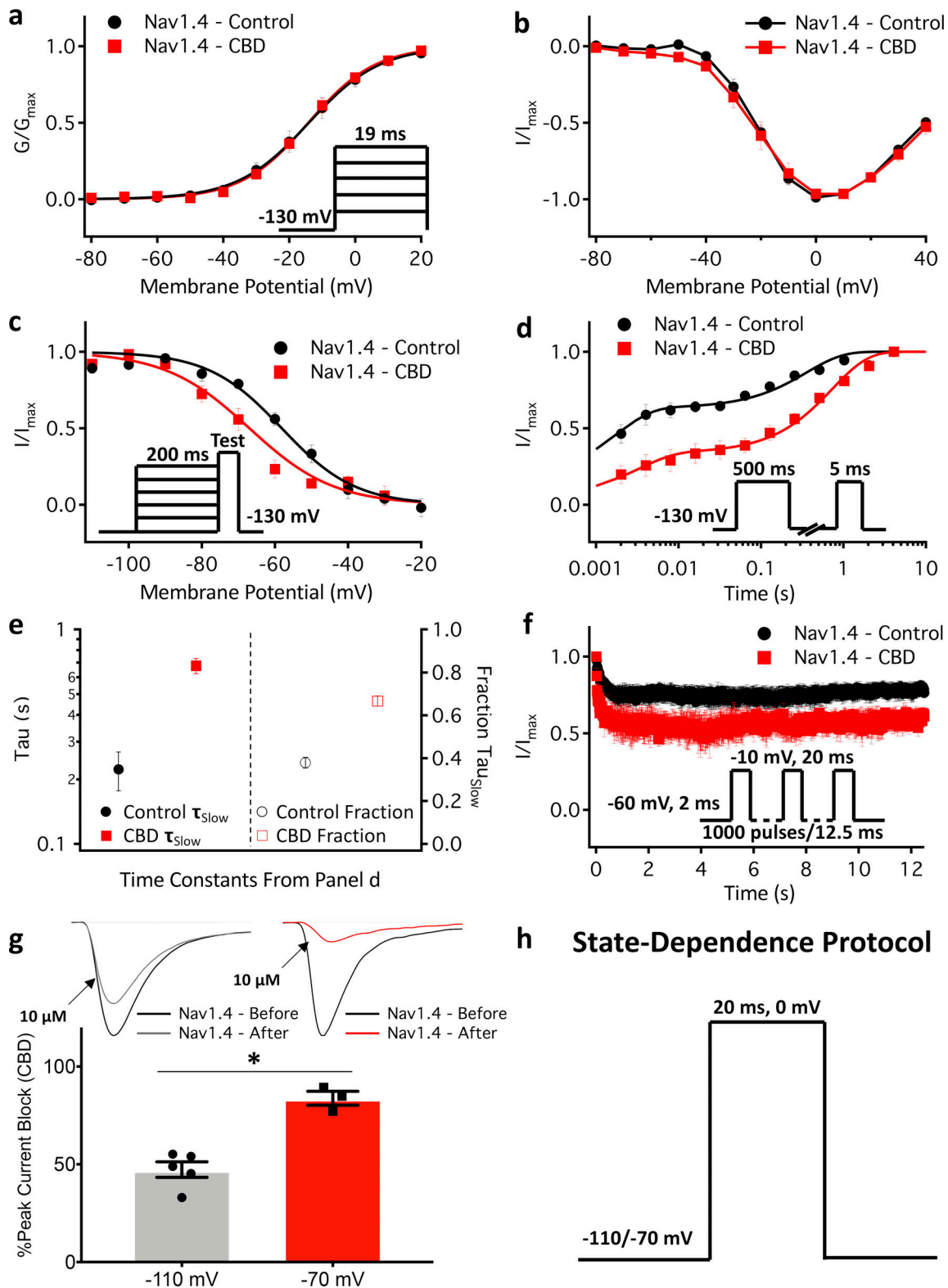


Figure 5. **Effects of CBD on Nav1.4 gating.** (a and b) Voltage dependence of activation as normalized conductance plotted against membrane potential in 1 μ M CBD (control: $V_{1/2} = -19.9 \pm 4.2$ mV, $z = 2.8 \pm 0.3$, $n = 5$; CBD: $V_{1/2} = -14.3 \pm 4.2$ mV, $z = 2.8 \pm 0.3$, $n = 5$; $P > 0.05$ for both $V_{1/2}$ and z) and normalized activating currents as a function of potential. (c) Voltage dependence of 200 ms (channels were held at -130 mV for 200 ms) F-I curve plotted against membrane potential in 1 μ M CBD (control: $V_{1/2} = -64.1 \pm 2.4$ mV, $z = -2.7 \pm 0.3$, $n = 8$; CBD: $V_{1/2} = -72.7 \pm 3.0$ mV, $z = -2.8 \pm 0.4$, $n = 5$; $P = 0.0281$ for $V_{1/2}$ and $P > 0.05$ for z). (d) Recovery from fast inactivation in 1 μ M CBD at 500 ms (control: $\tau_{Fast} = 0.0025 \pm 0.00069$ s, $\tau_{Slow} = 0.224 \pm 0.046$ s; $n = 7$; CBD: $\tau_{Fast} = 0.0048 \pm 0.00081$ s; $\tau_{Slow} = 0.677 \pm 0.054$ s; $n = 5$; $P = 0.0330$ for τ_{Fast} and $P < 0.0001$ for τ_{Slow}). (e) The slow components of recovery from inactivation in control and CBD (1 μ M) at 500 ms are shown on the left y axis on a logarithmic scale, and the fraction of slow to fast component of recovery from inactivation is

shown on the right y axis. **(f)** Use-dependent inactivation in control and 2 μM CBD. Normalized current decay plotted as a function of time fitted with an exponential curve (control: $\tau = 0.14 \pm 0.086$ s, $n = 6$; CBD: $\tau = 0.018 \pm 0.0028$ s, $n = 3$; $P < 0.05$). **(g)** State-dependent block of peak Nav1.4 current at 10 μM (-110 mV: mean block = $47.3 \pm 3.7\%$, $n = 5$; -70 mV: mean block = $83.8 \pm 3.6\%$, $n = 3$; *, $P = 0.0003$). **(h)** Pulse protocol used for state dependence experiments. Recordings were performed at 1 Hz. Error bars are SE in mean.

findings in Nav1.4, we compared the CBD-mediated (10 μM) peak current block from -110 and -70 mV holding potentials. We found that whereas 10 μM CBD blocked ~45% of the Nav1.4 current at -110 mV, it blocked ~84% of the current from -70 mV (Fig. 5, g and h).

Collectively, these results support our hypothesis that CBD nonselectively modulates Nav gating and further suggests how CBD may reduce Nav1.4 excitability. However, our results in this paper predominantly describe the CBD effects on fast inactivation and not slow inactivation.

CBD hyperpolarizes F-I curve in Nav1.4-WWWW

To determine a possible association between membrane elasticity and stabilized inactivation, we measured effects of CBD before and after compound perfusion in the WWWW mutant in a matched-pair manner. Although CBD did not inhibit peak I_{Na} , it hyperpolarized the F-I curve ($P < 0.05$), suggesting CBD's modulation of membrane elasticity could at least in part be responsible for stabilizing Nav inactivation (Fig. S9). This is an interesting finding because our GFA results suggest that CBD increases bilayer stiffness or thickness, and previous studies suggested that compounds such as Triton X-100 that reduce this stiffness or thickness also hyperpolarize the Nav F-I curve (Lundbæk et al., 2004). Therefore, it is also possible that the hyperpolarization of the F-I curve in WWWW could be due to a different and unrelated mechanism.

CBD effects on a pH-sensitive mixed myotonia/hypoPP Nav1.4 mutant, P1158S (DIII-S4-S5)

Because CBD is therapeutic against seizure disorders (Devinsky et al., 2017), typically considered neuronal GOF conditions, we examined whether CBD may similarly ameliorate a skeletal muscle GOF condition (Cannon, 2015). We recently discovered that the P1158S mutation in Nav1.4 increases the channel's pH sensitivity (Ghovanloo et al., 2018a). The P1158S gating displays pH-dependent shifts that, using AP modeling, are predicted to correlate with the phenotypes associated with this variant. Therefore, the relationship between pH and P1158S could be used as an *in vitro/in silico* assay of Nav1.4 hyperexcitability (to model moderate to severe GOF). Here, we used this assay to investigate CBD's effects on skeletal muscle hyperexcitability. We tested effects of 1 μM CBD (acid dissociation constant, 9.64) on P1158S at pH 6.4 (myotonia triggering) and pH 7.4 (hypoPP triggering). Fig. 6 shows CBD effects on P1158S at low and high pH. Interestingly, the lack of selectivity in gating modulation by CBD also exists in P1158S at both pHs. CBD did not change activation ($P > 0.05$), but it hyperpolarized inactivation ($P < 0.05$) and slowed recovery from inactivation ($P < 0.05$; Fig. 6, a-f). Consistent with previous results where CBD inhibited persistent I_{Na} (Ghovanloo et al., 2018c; Patel et al., 2016), CBD also reduced the exacerbated persistent I_{Na} associated with P1158S at pH 7.4

($P < 0.05$; Fig. 6 g). Persistent I_{Na} reduction could not be detected at pH 6.4 ($P > 0.05$; Fig. 6 h), because both low pH (Ghovanloo et al., 2018a, 2018b; Peters et al., 2018) and CBD reduce current amplitudes to levels where differences in amplitudes could not be resolved above background noise. Sample persistent currents are shown in Fig. 6, g and h.

AP model predicts that CBD reduces myotonia, also to a lesser extent periodic paralysis, in the P1158S-pH assay

We used the gating changes from the patch-clamp experiments with WT and P1158S (both control and 1 μM CBD) to model the skeletal muscle AP (Cannon et al., 1993; Ghovanloo et al., 2018a). We ran the simulations using a 50 $\mu\text{A}/\text{cm}^2$ stimulus. The simulation pulse started at 50 ms and stopped at 350 ms (Fig. 7). During this pulse, the WT channels activated at 50 ms and fired a single AP. The channels remained inactivated until the stimulus was removed at 350 ms, and then the membrane potential recovered back to its resting value (Fig. 7 a). CBD reduced the AP amplitude (Fig. 7 b), consistent with CBD effects observed in different neuron types (Khan et al., 2018; Ghovanloo et al., 2018c). At pH 6.4, P1158S displayed a continuous train of APs for the entire stimulation period. After the stimulus was removed, P1158S showed a progressive series of afterdepolarizations (or afterdischarges) of the membrane potential, characteristic of a myotonic burst (Fig. 7 c; Cannon, 2015). Interestingly, the CBD-mediated shifts at pH 6.4 in P1158S reduced the simulated AP amplitudes for the entirety of the pulse duration; delayed onset of the first AP, consistent with CBD preventing Nav opening (as shown by measurements on peak Nav conductance in Ghovanloo et al., 2018c); and abolished the postpulse myotonic afterdepolarizations (Fig. 7 d). At pH 7.4, P1158S fired a single AP, followed by a period where membrane potential remained depolarized around -35 mV even after stimulus termination (Fig. 7 e). This inability to repolarize holds the Navs in an inactivated state and is consistent with the periodic paralysis phenotype (Cannon, 2015). In contrast to the myotonic phenotype, CBD did not alleviate, to the same extent, the periodic paralysis phenotype in our P1158S-pH *in vitro/in silico* assay (Fig. 7 f).

CBD reduces rat diaphragm muscle contraction at saturating concentrations

To survey and determine whether CBD reduces skeletal muscle contractions, we surgically removed rat diaphragm muscles and measured muscle contractions evoked by phrenic nerve stimulation. In Fig. 8, a and b, we show images of the diaphragm cut into a hemidiaphragm. We used electrodes to stimulate the phrenic nerve and measured the muscle contraction using a force transducer at a saturating concentration of 100 μM CBD, reasoning that if CBD reduces muscle contraction, a saturating concentration should provide a large enough response to detect

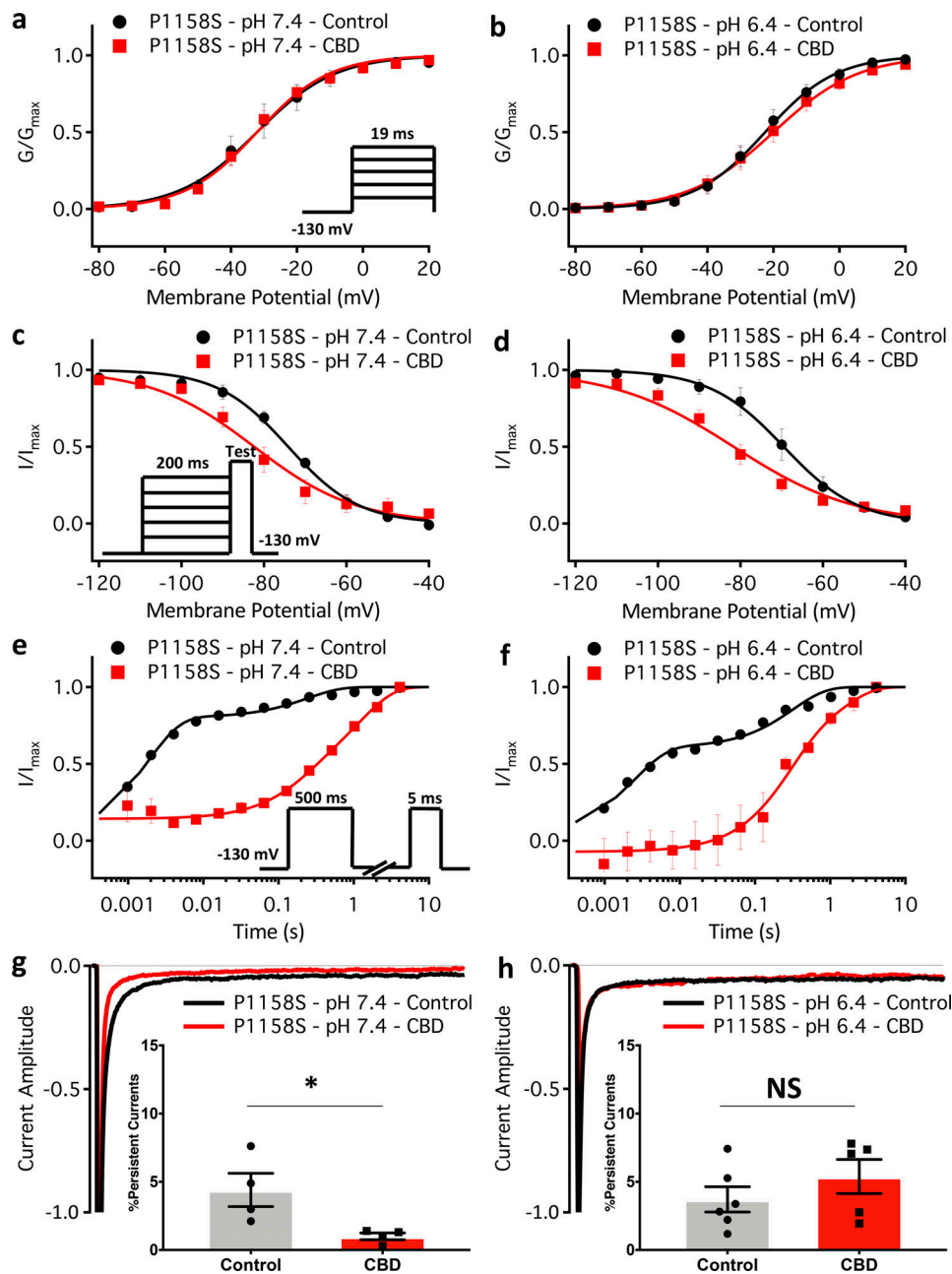
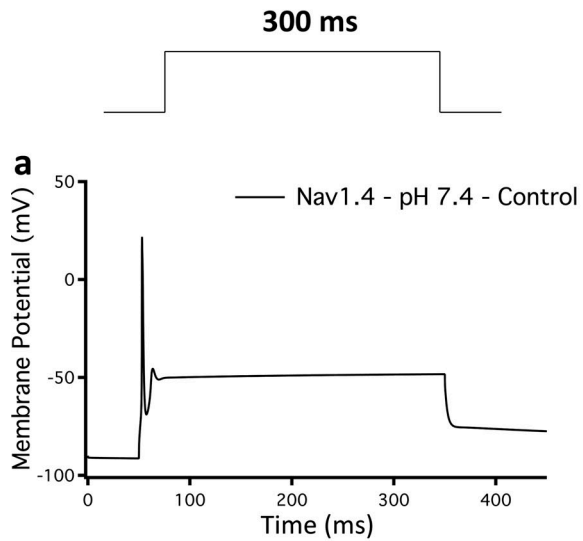


Figure 6. Effects of CBD (1 μM) on gating of a myotonia/hypoPP variant, P1158S. (a and b) Voltage dependence of activation as normalized conductance plotted against membrane potential at pH 7.4 (control: $V_{1/2} = -30.0 \pm 3.3$ mV, $z = 3.1 \pm 0.2$, $n = 8$; CBD: $V_{1/2} = -32.7 \pm 3.6$ mV, $z = 2.9 \pm 0.2$, $n = 7$; $P > 0.05$ for both $V_{1/2}$ and z) and pH 6.4 (control: $V_{1/2} = -23.0 \pm 3.3$ mV, $z = 2.9 \pm 0.2$, $n = 8$; CBD: $V_{1/2} = -21.1 \pm 3.3$ mV, $z = 2.5 \pm 0.2$, $n = 8$; $P > 0.05$ for both $V_{1/2}$ and z). (c and d) Voltage dependence of 200-ms F-I curve plotted against membrane potential (channels were held at -130 mV for 200 ms) at pH 7.4 (control: $V_{1/2} = -73.2 \pm 2.6$ mV, $z = 2.9 \pm 0.2$, $n = 7$; CBD: $V_{1/2} = -83.0 \pm 2.6$ mV, $z = 3.0 \pm 0.3$; $P = 0.0260$ for $V_{1/2}$ and $P > 0.05$ for z) and pH 6.4 (control: $V_{1/2} = -68.4 \pm 3.0$ mV, $z = 2.7 \pm 0.4$, $n = 5$; CBD: $V_{1/2} = -81.7 \pm 2.3$ mV, $z = 2.7 \pm 0.3$, $n = 9$; $P = 0.0010$ for $V_{1/2}$ and $P > 0.05$ for z). (e and f) Recovery from fast inactivation at 500 ms at pH 7.4 (control: $\tau_{Fast} = 0.0018 \pm 0.006$ s, $\tau_{Slow} = 0.15 \pm 0.6$ s, $n = 7$; CBD: $\tau_{Fast} = 0.24 \pm 0.07$ s; $\tau_{Slow} = 2.5 \pm 0.6$ s, $n = 6$; $P = 0.0347$ for τ_{Fast} and $P = 0.0245$ for τ_{Slow}) and pH 6.4 (control: $\tau_{Fast} = 0.065 \pm 0.04$ s, $\tau_{Slow} = 0.75 \pm 0.4$ s, $n = 7$; CBD: $\tau_{Fast} = 0.13 \pm 0.07$ s; $\tau_{Slow} = 0.62 \pm 0.1$ s, $n = 4$; $P < 0.05$ for τ_{Fast} and $P > 0.05$ for τ_{Slow}). (g and h) Persistent currents measured from a 200-ms depolarizing pulse to 0 mV from a holding potential of -130 mV at pH 7.4 (control: percentage = $4.4 \pm 1.2\%$, $n = 4$; CBD: percentage = $1.0 \pm 0.2\%$, $n = 4$; *, $P = 0.0339$; $n = 4$) and pH 6.4 (control: percentage = $4.4 \pm 2.1\%$, $n = 6$; CBD: percentage = $5.4 \pm 1.2\%$, $n = 5$; $P > 0.05$). Error bars are SE in mean.

any potential reduction in contraction. Our results suggested that CBD reduces the contraction amplitude to ~60% of control ($P < 0.05$; Fig. 8 c). Next, we sought to determine whether a selective block of Nav channels also reduces skeletal muscle contraction using 300 nM TTX, a saturating concentration of

this potent blocker of selected Nav channels ($IC_{50} \sim 10\text{--}30$ nM on TTX-sensitive channels; Hille, 2001). TTX also reduced contraction to ~20% of control ($P < 0.05$; Fig. 8 c). The remaining ~20% contraction could be due to stimulation of voltage-gated calcium channels in transverse membranes that directly interact

Pulse Protocol



P1158S-pH – Skeletal Muscle Hyperexcitability Assay

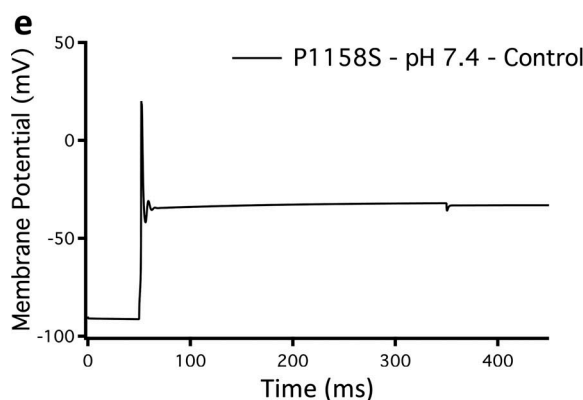
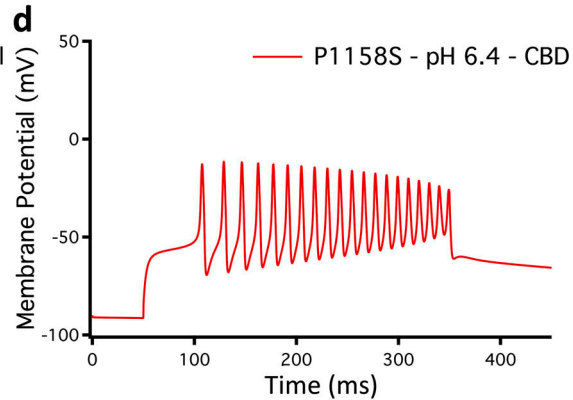
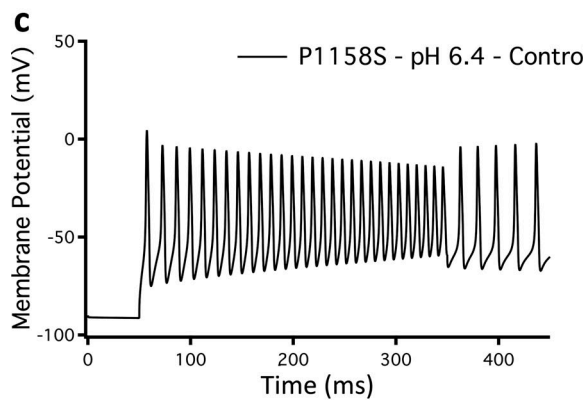
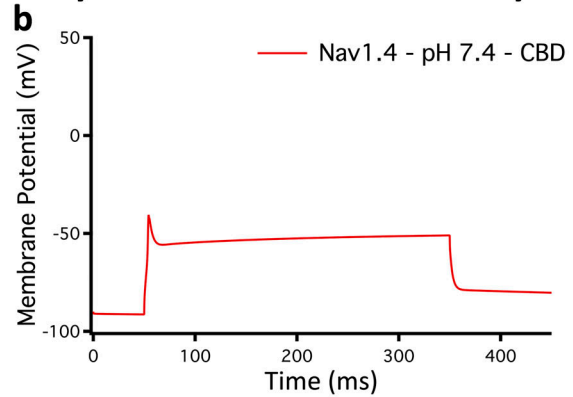
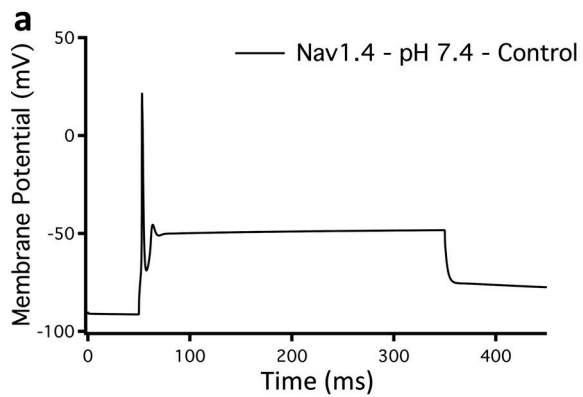
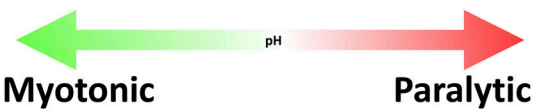


Figure 7. **AP simulations of skeletal muscle APs in the presence and absence of CBD, based on voltage-clamp data.** Top of the figure shows the pulse protocol used for simulations, and a cartoon representation of P1158S-pH *in vitro/in silico* assay, where pH can be used to control the P1158S phenotype. **(a and b)** Simulations in WT-Nav1.4 in the presence and absence of CBD. **(c and d)** Simulations of P1158S at pH6.4. **(e and f)** Results from pH 7.4.

with ryanodine-sensitive calcium release in the SR that can initiate contraction (Catterall, 2011; Tanabe et al., 1993; Catterall, 1991). Representative traces of muscle contraction in control, CBD, and TTX are shown in Fig. 8, d-f. These results show that a selective inhibition of Nav reduces skeletal muscle contraction, which suggests that CBD's reduction of muscular contraction could be due, at least in part, to its effect on Nav (Ghovanloo et al., 2018c). Therefore, our

molecular *in vitro* and *in silico* data could have some physiological relevance.

Discussion

Proposed pathway and mechanism of Nav1.4 inhibition by CBD
Although CBD holds therapeutic promise (Devinsky et al., 2017; Ghovanloo et al., 2018c; Kaplan et al., 2017; Patel et al., 2016; Ross

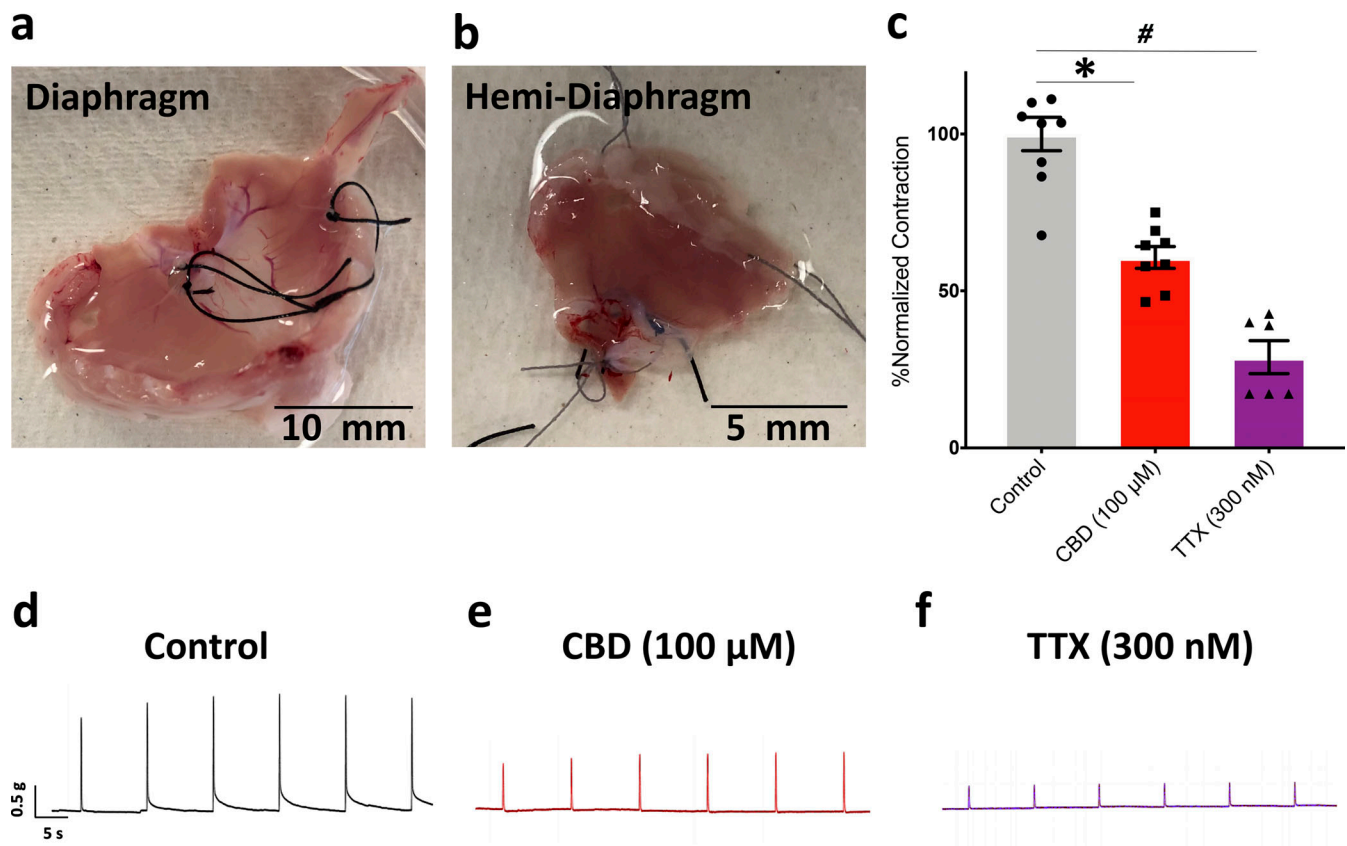


Figure 8. **Effects of CBD on rat diaphragm contraction.** (a) Image of dissected rat diaphragm muscle. (b) Image of rat diaphragm cut into a hemidiaphragm, which was placed between electric plates that were used for electric stimulation. The subsequent muscle contractions were measured using a force transducer. (c) Normalized quantification of muscle contractions in CBD and TTX (percentage of normalized contraction: control = $100 \pm 5.3\%$, $n = 9$; CBD = $60.6 \pm 3.5\%$, $n = 8$; TTX = $28.9 \pm 5.3\%$, $n = 6$; * indicates $P = 0.0006$ for CBD; # indicates $P < 0.0001$ for TTX). Error bars are SE in mean. (d–f) Sample contraction traces across all three conditions.

et al., 2008; Pumroy et al., 2019; Fouda et al., 2020) and has been approved for two seizure disorders, its mechanisms of action remain largely unknown. We previously described the effects of CBD on Navs, which are among its proposed targets (Ghovanloo et al., 2018c). CBD's effects on neuronal Navs resemble the properties described for both amphiphilic compounds and traditional pore blockers. That study provided foundational hypotheses about CBD's mechanism of action on Navs. Here, we tested those ideas using a combination of in vitro, in silico, and ex vivo techniques.

Amphiphiles, molecules possessing both hydrophobic and hydrophilic properties, often display nonselective modulatory effects on seemingly unrelated targets (Lundbæk et al., 2004, 2005; Chisari et al., 2010; Kapoor et al., 2019). The apparent diversity of targets is a by-product of amphiphiles modulating membrane elasticity (Lundbæk et al., 2004, 2005; Rusinova et al., 2011; Kapoor et al., 2019). This modification is achieved by amphiphiles localizing at the solution–bilayer interface, which is possible by having the compound's polar group residing at the interface with the hydrophobic region, which then gets inserted into the bilayer core. This partitioning into the lipid bilayer alters membrane elasticity and changes phase preference and curvature (Lundbæk et al., 2004, 2005; Kapoor et al., 2019). The net effect of these alterations to the membrane for the

bilayer-embedded Nav channel is to stabilize the inactivated state (Lundbæk et al., 2004, 2005; Rusinova et al., 2011; Kapoor et al., 2019).

We used MD simulations to “visualize” CBD localization and its effects on the membrane. Interestingly, the MD prediction regarding localization, independently confirmed by NMR measurements of CBD in lipid vesicles, suggested CBD positioning between C8 and C10. Our GFA findings suggested that CBD changes membrane elasticity in a concentration-dependent manner (1–30 μM), consistent with our previous findings, including CBD's temperature dependence (CBD effects were enhanced at lower temperatures), stabilization of Nav inactivation, and nonselectivity of Nav inhibition (Ghovanloo et al., 2018c). Together, these results suggest that CBD inhibition of Nav currents (and possibly other ionic currents) is, at least in part, mediated through changing lipid bilayer elasticity. However, although we were able to detect a difference in gramicidin signal at the lowest CBD concentration (1–3 μM) compared with no CBD (0 μM; Fig. 2, b–d), we cannot unequivocally state whether the minimally induced stiffening of the membrane at lower CBD concentration is physiologically relevant.

We further found that CBD had the opposite effect to Triton X-100 in GFA. Also, the magnitude of change of the quench rate was different between the two compounds at a given

concentration; however, both compounds similarly hyperpolarized the Nav inactivation. These findings suggest that there may be two, possibly three, mechanisms involved. The exact mechanisms through which CBD's presence may alter the lipid-Nav interactions should be further investigated in future studies. One potential consideration would be an expectation of direct gramicidin-CBD interactions in GFA. However, the gramicidin channel structure provides no evidence for a binding site, and studies on many different molecules have shown that they alter the function of both left- and right-handed channels (see Kapoor et al., 2019). We are not aware of evidence for specific drug-gramicidin channel interactions, and therefore we think gramicidin-CBD interactions in GFA are unlikely.

The modulated receptor hypothesis suggests that resting-state block occurs when a compound enters from the lipid phase of the membrane into the LA binding site, whereas rapid open-state block happens when a compound enters the open pore from the cytosol (Hille, 1977; Hondeghem and Katzung, 1984). Pore blockers can reach their binding site from the cytosolic side when the activation gate (V-gate) is open. A recent study showed that compounds can have direct access from the membrane phase to the LA site through channel fenestrations, culminating in resting-state block (Gamal El-Din et al., 2018). We previously found that, after an over-time incubation of Nav channels in CBD (without pulsing), the first depolarizing pulse from -110 mV showed peak current block, suggesting that CBD could impart resting-state block (Ghovanloo et al., 2018c).

We previously found that some characteristics of CBD inhibition of Navs are similar to classic pore blockers (Ghovanloo et al., 2018c). Here, we tested CBD interactions inside the Nav1.4 LA site at rest. Destabilizing the LA site by the F1586A mutation reduced CBD block of Nav1.4. This result is particularly notable because the LA site becomes a more favorable interaction site when the channel adopts a more inactivated state (a key reason for LAs' strong state dependence; Ghovanloo and Ruben, 2020). Therefore, CBD's reduced block in F1586A at rest could support the idea that CBD interacts with Nav at the pore. However, this does not indicate that the pore is the primary determinant of CBD inhibition, especially when CBD is compared with a traditional blocker such as lidocaine, which is more affected by the F1586A mutation. However, it is also possible that CBD's interaction is merely less dependent on F1586 than lidocaine, with the pore LA site being equally critical for both compounds. This is supported by our recent CBD-NavM structure showing CBD's binding site is near to, but not identical with, known analgesic binding sites in Nav channels (Sait et al., 2020). An alternative explanation for the difference in CBD inhibition of WT versus F1586A could be differences in inactivated state occupancy; however, based on our computational (Figs. 3, 4, S2, and S3) and previously published structural data (Sait et al., 2020), we think that this explanation is less likely.

Next, we reasoned that, if CBD blocks the pore, a likely path to reach the pore from the lipid phase would be through the Nav fenestrations (based on MD results, high LogP, and high lipid binding partitioning). A previous study determined that reducing the diameter of NavAb (sodium channel from *Arcobacter butzleri*) fenestrations reduces access to both lidocaine and

flecainide size dependently into the channel pore, as shown by measuring the peak current amplitude after compound wash and with the first pulse from rest (Gamal El-Din et al., 2018). Here, we found that our fenestration-altered Nav1.4-WWWW construct abolished resting-state block by CBD, but not lidocaine or flecainide, after compounds reached equilibrium. This could be a consequence of the differences in hydrophobicity (and size/shape) between these three compounds. Because CBD is several orders of magnitude more hydrophobic than either lidocaine or flecainide, it may preferentially reach the pore through the fenestrations, whereas lidocaine and flecainide can reach the pore also from the cytoplasmic phase even if access through the fenestrations is blocked. This interpretation is consistent with the modulated receptor hypothesis (Fig. S10). Because the WWWW construct produced small currents, we could not dissect out the passage of lidocaine/flecainide through the fenestrations or the cytosolic V-gate, which requires having large currents to detect I_{Na} reduction at the first pulse after compound perfusion (Hille, 1977; Gamal El-Din et al., 2018). Once equilibrium is reached, even if the pathway through the fenestrations is altered, the pathway through the V-gate allows compound passage into the channel pore. This could conceivably be achieved if the compound were sufficiently hydrophilic to interact with the aqueous cytosolic side.

Our functional and computational results in this study, along with previous structural findings describing the CBD binding inside the NavM pore (Sait et al., 2020) at the fenestration-pore interface, suggest that the CBD pathway of I_{Na} block is most likely through the intramembrane lipid phase.

Finally, we determined that while I_{Na} block by CBD seems to occur through its interactions inside the Nav1.4 pore, its stabilization of inactivation could at least in part arise from modulating membrane elasticity; however, the exact nature and mechanism through which this inactivation stabilization occurs remains unresolved. Both mechanisms of pore block and stabilization of inactivation appear to contribute to the inhibition of Nav currents by CBD.

Possible clinical applications for CBD in skeletal muscle disorders

Skeletal muscle hyperexcitability disorders have historically received less attention than disorders in other tissues, including the brain. Drugs most commonly used for myotonia include compounds developed for other conditions, such as anti-convulsants and antiarrhythmics (Alfonsi et al., 2007; Trip et al., 2008), which may cause unwanted, off-target side effects. Hence, another therapeutic approach has been lifestyle modifications. For instance, myotonic patients may modify their lifestyles to avoid triggers such as potassium ingestion or cold temperatures. Treatment of hypoPP is usually achieved using oral potassium ingestion and by avoiding dietary carbohydrates and sodium. During hypokalemia, increasing K^+ levels may reduce membrane depolarization and shift the resting potential to more negative potentials. Acetazolamide or dichlorphenamide may be useful; however, these compounds can exacerbate symptoms (Torres et al., 1981; Tawil et al., 2000; Sternberg et al., 2001; Venance et al., 2004). There is a need for new treatments for these conditions.

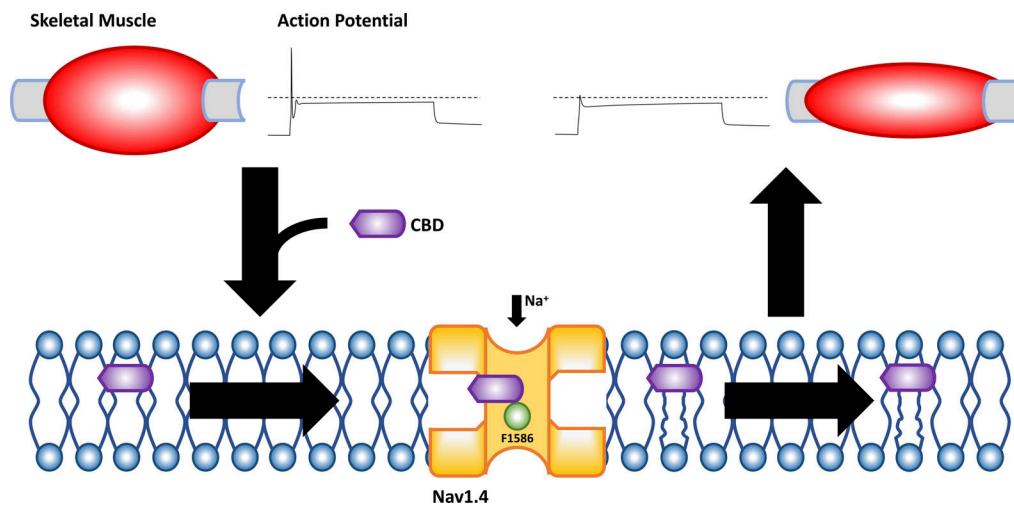


Figure 9. **Pathway of skeletal muscle inhibition via Nav1.4.** This is a cartoon representation of the mechanism and pathway through which CBD inhibits Nav1.4. Once CBD is exposed to the skeletal muscle, given its high lipophilicity, the majority of it gets inside the sarcolemma. Upon entering the sarcolemma, it localizes in the middle regions of the leaflet and travels through the Nav1.4 fenestrations into the pore. Inside the pore mutation of the LA, F1586A reduces CBD inhibition. CBD also alters the membrane elasticity, which promotes the inactivated state of the Nav channel, which adds to the overall CBD inhibitory effects. The net result is a reduced electrical excitability of the skeletal muscle, which, at least in part, contributes to a reduction in muscle contraction.

Cannabinoids have long been used to alleviate muscular problems (Borgelt et al., 2013; Baker et al., 2000). In this study, we show that CBD reduces skeletal contraction in rat diaphragm muscle. As CBD is a polypharmacology compound, we cannot state with certainty that the observed contraction reduction is due to I_{Na} inhibition alone, but, as demonstrated with the TTX results, I_{Na} block is sufficient to reduce contraction, meaning that CBD's activity at Nav1.4 could be a part of the mechanism in this reduction. Another caveat is that we cannot exclude the possibility of a phrenic nerve-independent (i.e., direct muscle) stimulation resulting in muscle contraction in our myography experiments. Although our results show that 100 μ M CBD reduces muscular contraction in our ex vivo experiments, 100 μ M is orders of magnitude higher than clinically achievable CBD concentrations in humans or rodents (Devinsky et al., 2017; Deiana et al., 2012). Our goal in performing these ex vivo experiments was merely to survey whether CBD reduces isolated muscular contraction; however, any potential clinical merits for CBD against muscle contractility hyperexcitability should be investigated in future clinically oriented (and/or in vivo) studies, as the primary focus of the present study was to investigate the molecular effects of CBD on Nav1.4. The overall mechanism suggested by our results is summarized in Fig. 9.

To explore a possible use for CBD in myotonia and hypoPP, we tested it in an in vitro/in silico assay. Our results suggest that CBD may alleviate myotonia but not the hypoPP phenotype (at least not to the same extent). One caveat is that these predictions are based in part on computer simulations. However, from a theoretical perspective, most Nav1.4 mutations that cause myotonia do so by changing conventional channel gating (e.g., activation, inactivation, persistent currents); hypoPP mutants are due to pathogenic gating pore currents associated with the VSD, so it is conceivable that a compound such as CBD may alleviate myotonic behavior without reducing hypoPP.

Potential adverse consequences of CBD

The structural similarities in the Nav family are a major challenge in developing selective Nav-targeting therapeutics (Ahuja et al., 2015; Bankar et al., 2018). Most small molecules that inhibit Nav channels are nonselective in nature, a function of the binding site in the pore of the channel in which key residues are conserved across the orthologues. Despite this lack of selectivity, these molecules have found wide-ranging clinical efficacy in disorders of excitability (Hondegheem and Katzung, 1984; Mantegazza et al., 2010). However, these compounds typically have a narrow therapeutic index, presumably due to their nonselective inhibition.

Previous behavior-related studies in rodents suggest that CBD's efficacious plasma levels are within the 6.8–8.3 μ M range (Deiana et al., 2012). This concentration range is approximately the window at which CBD has been shown to modulate various targets (including Navs) and also to modulate membrane elasticity (Fig. 2 and Table 1). The combined results described in this paper and our other recent studies (Ghovanloo et al., 2018c; Fouda et al., 2020; Sait et al., 2020) suggest that CBD, as a Nav inhibitor, would suffer from the same limitations as traditional Nav blockers. Furthermore, at least in part because of its hydrophobicity, CBD modulates a wider range of targets than traditional Nav blockers (Ghovanloo et al., 2018c; Ross et al., 2008; Pumroy et al., 2019). These properties could cause enough off-target effects to render CBD useless against Nav hyperexcitable conditions, including the conditions associated with the skeletal muscle. However, the strongest argument for CBD as a Nav-related therapeutic is its clinically proven efficacy in Dravet syndrome. This efficacy is likely the result of CBD modulating multiple targets and not just one particular set of Nav channels (Devinsky et al., 2017).

Conclusion

In conclusion, our results suggest that CBD inhibition of Nav has at least two components: altered membrane elasticity and pore

Table 1. Overview of some of the main CBD molecular targets^a

Molecular target	Effect	References
CB1	Antagonist, negative allosteric modulator	Laprairie et al., 2015; Thomas et al., 2007
CB2	Antagonist	Thomas et al., 2007
Nav channels	Inhibitor	Ghovanloo et al., 2018c; Sait et al., 2020
Kv2.1 channel	Inhibitor	Ghovanloo et al., 2018c
Cav channels	Inhibitor	Deiana et al., 2012; Ross et al., 2008
TRPV channels	Agonist	Galaj et al., 2020; Bisogno et al., 2001; Pumroy et al., 2019
GPR55	Antagonist	Harding et al., 2018; Kaplan et al., 2017
Lipid membrane	Decreases elasticity	This study

Cav, voltage-gated calcium channel; GPR55, G protein-coupled receptor 55; Kv2.1, voltage-gated potassium channel; TRPV, transient receptor potential cation channel.

^aSee de Almeida and Devi (2020) for a more extensive review of CBD targets and signaling pathways.

block. Nav1.4 inhibition could contribute to CBD reducing skeletal muscle contractions and may have potential therapeutic value against myotonia and possibly, to a lesser extent, against periodic paralysis (Fig. 9). From a broader perspective, our proposed mechanism may hold true for other compounds that are similar to CBD in modulating Navs or other channels with similar structures.

Acknowledgments

Christopher J. Lingle served as editor.

We thank Drs. Colin Peters, Eric Lin, and Nina Weishaupt for their contributions. The MD simulations were performed with resources provided by the Swedish National Infrastructure for Computing at PDC Center for High Performance Computing.

This work was supported by grants from the Natural Science and Engineering Research Council of Canada and the Rare Disease Foundation to P.C. Ruben and M.-R. Ghovanloo (Canada Graduate Scholarships-Doctoral 535333-2019 and Michael Smith Foreign Study Supplements 546467-2019, respectively), a Mitacs Accelerate fellowship in partnership with Xenon Pharma, Inc. to M.-R. Ghovanloo (IT10714), a Mitacs Elevate fellowship in partnership with Akseera Pharma, Inc. to M.A. Fouda, grants from SciLifeLab and the Swedish Research Council to L. Delemotte (VR 2018-04905), and a grant from the National Institutes of Health to O.S. Andersen (GM021342).

The authors declare no competing financial interests.

Author contributions: M.-R. Ghovanloo assembled data; performed patch-clamp experiments; assisted in ITC experiments, AP modeling/simulations, functional assay development, data analysis, and figure making; wrote the manuscript; interpreted data; and assisted with conceiving of experiments. K.

Choudhury and T.S. Bandaru performed MD simulations and docking. M.A. Fouda performed myography. K. Rayani performed ITC and assisted in mutagenesis and various experimental conceptualizations. R. Rusinova performed GFA. T. Phaterpekar performed NMR. K. Nelkenbrecher performed diaphragm preparation. A.R. Watkins helped with NMR. D. Pobjurko assisted with myography. J. Thewalt, O.S. Andersen, L. Delemotte, S.J. Goodchild, and P.C. Ruben conceived the experiments and revised the manuscript critically. All coauthors edited the manuscript.

Submitted: 8 July 2020

Revised: 13 December 2020

Accepted: 16 March 2021

References

- Abraham, M.J., T. Murtola, R. Schulz, S. Páll, J.C. Smith, B. Hess, and E. Lindahl. 2015. GROMACS: High performance molecular simulations through multi-level parallelism from laptops to supercomputers. *SoftwareX*. 1-2:19-25. <https://doi.org/10.1016/j.softx.2015.06.001>
- Ahuja, S., S. Mukund, L. Deng, K. Khakh, E. Chang, H. Ho, S. Shriver, C. Young, S. Lin, J.P. Johnson Jr., et al. 2015. Structural basis of Nav1.7 inhibition by an isoform-selective small-molecule antagonist. *Science*. 350:aac5464. <https://doi.org/10.1126/science.aac5464>
- Alfonsi, E., I.M. Merlo, M. Tonini, S. Ravaglia, R. Brugnoli, A. Gozzini, and A. Moglia. 2007. Efficacy of propafenone in paramyotonia congenita. *Neurology*. 68:1080-1081. <https://doi.org/10.1212/01.wnl.0000257825.29703.e8>
- Andersen, O.S., and R.E. Koeppe II. 2007. Bilayer thickness and membrane protein function: an energetic perspective. *Annu. Rev. Biophys. Biomol. Struct.* 36:107-130. <https://doi.org/10.1146/annurev.biophys.36.040306.132643>
- Baker, D., G. Pryce, J.L. Croxford, P. Brown, R.G. Pertwee, J.W. Huffman, and L. Layward. 2000. Cannabinoids control spasticity and tremor in a multiple sclerosis model. *Nature*. 404:84-87. <https://doi.org/10.1038/35003583>
- Bankar, G., S.J. Goodchild, S. Howard, K. Nelkenbrecher, M. Waldbrook, M. Dourado, N.G. Shuart, S. Lin, C. Young, Z. Xie, et al. 2018. Selective Nav1.7 antagonists with long residence time show improved efficacy against inflammatory and neuropathic pain. *Cell Rep.* 24:3133-3145. <https://doi.org/10.1016/j.celrep.2018.08.063>
- Bean, B.P., C.J. Cohen, and R.W. Tsien. 1983. Lidocaine block of cardiac sodium channels. *J. Gen. Physiol.* 81:613-642. <https://doi.org/10.1085/jgp.81.5.613>
- Bisogno, T., L. Hanuš, L. De Petrocellis, S. Tchilibon, D.E. Ponde, I. Brandi, A.S. Moriello, J.B. Davis, R. Mechoulam, and V. Di Marzo. 2001. Molecular targets for cannabidiol and its synthetic analogues: effect on vanilloid VR1 receptors and on the cellular uptake and enzymatic hydrolysis of anandamide. *Br. J. Pharmacol.* 134:845-852. <https://doi.org/10.1038/sj.bjpp.0704327>
- Borgelt, L.M., K.L. Franson, A.M. Nussbaum, and G.S. Wang. 2013. The pharmacologic and clinical effects of medical cannabis. *Pharmacotherapy*. 33:195-209. <https://doi.org/10.1002/phar.1187>
- Buchanan, J.T. 1993. Electrophysiological properties of identified classes of lamprey spinal neurons. *J. Neurophysiol.* 70:2313-2325. <https://doi.org/10.1152/jn.1993.70.6.2313>
- Bülbring, E. 1946. Observations on the isolated phrenic nerve diaphragm preparation of the rat. *Br. J. Pharmacol. Chemother.* 1:38-61. <https://doi.org/10.1111/j.1476-5381.1946.tb00025.x>
- Cannon, S.C. 2006. Pathomechanisms in channelopathies of skeletal muscle and brain. *Annu. Rev. Neurosci.* 29:387-415. <https://doi.org/10.1146/annurev.neuro.29.051605.112815>
- Cannon, S.C. 2015. Channelopathies of skeletal muscle excitability. *Compr. Physiol.* 5:761-790. <https://doi.org/10.1002/cphy.c140062>
- Cannon, S.C., R.H. Brown Jr., and D.P. Corey. 1993. Theoretical reconstruction of myotonia and paralysis caused by incomplete inactivation of sodium channels. *Biophys. J.* 65:270-288. [https://doi.org/10.1016/S0006-3495\(93\)81045-2](https://doi.org/10.1016/S0006-3495(93)81045-2)

- Catterall, W.A. 1991. Excitation-contraction coupling in vertebrate skeletal muscle: a tale of two calcium channels. *Cell*. 64:871–874. [https://doi.org/10.1016/0092-8674\(91\)90309-M](https://doi.org/10.1016/0092-8674(91)90309-M)
- Catterall, W.A. 2011. Voltage-gated calcium channels. *Cold Spring Harb. Perspect. Biol.* 3:a003947. <https://doi.org/10.1101/cshperspect.a003947>
- Catterall, W.A. 2012. Voltage-gated sodium channels at 60: structure, function and pathophysiology. *J. Physiol.* 590:2577–2589. <https://doi.org/10.1113/jphysiol.2011.224204>
- Chisari, M., H.J. Shu, A. Taylor, J.H. Steinbach, C.F. Zorumski, and S. Mennerick. 2010. Structurally diverse amphiphiles exhibit biphasic modulation of GABA_A receptors: similarities and differences with neurosteroid actions. *Br. J. Pharmacol.* 160:130–141. <https://doi.org/10.1111/j.1476-5381.2010.00679.x>
- de Almeida, D.L., and L.A. Devi. 2020. Diversity of molecular targets and signaling pathways for CBD. *Pharmacol. Res. Perspect.* 8:e00682. <https://doi.org/10.1002/prp2.682>
- Deiana, S., A. Watanabe, Y. Yamasaki, N. Amada, M. Arthur, S. Fleming, H. Woodcock, P. Dorward, B. Pigliacampo, S. Close, et al. 2012. Plasma and brain pharmacokinetic profile of cannabidiol (CBD), cannabidivarin (CBDV), Δ⁹-tetrahydrocannabinol (THC) and cannabigerol (CBG) in rats and mice following oral and intraperitoneal administration and CBD action on obsessive-compulsive behaviour. *Psychopharmacology (Berl.)*. 219:859–873. <https://doi.org/10.1007/s00213-011-2415-0>
- De Petrocellis, L., A. Ligresti, A.S. Moriello, M. Allarà, T. Bisogno, S. Petrosino, C.G. Stott, and V. Di Marzo. 2011. Effects of cannabinoids and cannabinoid-enriched *Cannabis* extracts on TRP channels and endocannabinoid metabolic enzymes. *Br. J. Pharmacol.* 163:1479–1494. <https://doi.org/10.1111/j.1476-5381.2010.01166.x>
- Desaphy, J.-F., A. De Luca, M.P. Didonna, A.L. George Jr., and D. Camerino Conte. 2004. Different flecainide sensitivity of hNav1.4 channels and myotonic mutants explained by state-dependent block. *J. Physiol.* 554: 321–334. <https://doi.org/10.1113/jphysiol.2003.046995>
- Devinsky, O., J.H. Cross, L. Laux, E. Marsh, I. Miller, R. Nabbout, I.E. Scheffer, E.A. Thiele, and S. Wright. Cannabidiol in Dravet Syndrome Study Group. 2017. Trial of cannabidiol for drug-resistant seizures in the Dravet syndrome. *N. Engl. J. Med.* 376:2011–2020. <https://doi.org/10.1056/NEJMoa1611618>
- Devinsky, O., A.D. Patel, J.H. Cross, V. Villanueva, E.C. Wirrell, M. Privitera, S.M. Greenwood, C. Roberts, D. Checketts, K.E. VanLandingham, and S.M. Zuberi. GWPCARE3 Study Group. 2018. Effect of cannabidiol on drop seizures in the Lennox-Gastaut syndrome. *N. Engl. J. Med.* 378: 1888–1897. <https://doi.org/10.1056/NEJMoa1714631>
- Eijkelkamp, N., J.E. Linley, M.D. Baker, M.S. Minett, R. Cregg, R. Werdehausen, F. Rugiero, and J.N. Wood. 2012. Neurological perspectives on voltage-gated sodium channels. *Brain*. 135:2585–2612. <https://doi.org/10.1093/brain/aws225>
- Emery, A.E.H. 1991. Population frequencies of inherited neuromuscular diseases—a world survey. *Neuromuscul. Disord.* 1:19–29. [https://doi.org/10.1016/0960-8966\(91\)90039-U](https://doi.org/10.1016/0960-8966(91)90039-U)
- Featherstone, D.E., J.E. Richmond, and P.C. Ruben. 1996. Interaction between fast and slow inactivation in Skm1 sodium channels. *Biophys. J.* 71: 3098–3109.
- Fontaine, B. 2008. Periodic paralysis. *Adv. Genet.* 63:3–23. [https://doi.org/10.1016/S0065-2660\(08\)01001-8](https://doi.org/10.1016/S0065-2660(08)01001-8)
- Fouda, M.A., M.-R. Ghovanloo, and P.C. Ruben. 2020. Cannabidiol protects against high glucose-induced oxidative stress and cytotoxicity in cardiac voltage-gated sodium channels. *Br. J. Pharmacol.* 177:2932–2946. <https://doi.org/10.1111/bph.15020>
- Galaj, E., G.H. Bi, H.J. Yang, and Z.X. Xi. 2020. Cannabidiol attenuates the rewarding effects of cocaine in rats by CB2, 5-HT_{1A} and TRPV1 receptor mechanisms. *Neuropharmacology*. 167:107740. <https://doi.org/10.1016/j.neuropharm.2019.107740>
- Gamal El-Din, T.M., M.J. Linaeus, N. Zheng, and W.A. Catterall. 2018. Fenestrations control resting-state block of a voltage-gated sodium channel. *Proc. Natl. Acad. Sci. USA*. 115:13111–13116. <https://doi.org/10.1073/pnas.1814928115>
- Ghovanloo, M.-R., and P.C. Ruben. 2020. Say cheese: structure of the cardiac electrical engine is captured. *Trends Biochem. Sci.* 45:369–371. <https://doi.org/10.1016/j.tibs.2020.02.003>
- Ghovanloo, M.-R., K. Aimar, R. Ghadir-Tavi, A. Yu, and P.C. Ruben. 2016. Physiology and pathophysiology of sodium channel inactivation. *Curr. Top. Membr.* 78:479–509. <https://doi.org/10.1016/bs.ctm.2016.04.001>
- Ghovanloo, M.-R., M. Abdelsayed, C.H. Peters, and P.C. Ruben. 2018a. A mixed periodic paralysis & myotonia mutant, P1158S, imparts pH-sensitivity in skeletal muscle voltage-gated sodium channels. *Sci. Rep.* 8:6304. <https://doi.org/10.1038/s41598-018-24719-y>
- Ghovanloo, M.-R., C.H. Peters, and P.C. Ruben. 2018b. Effects of acidosis on neuronal voltage-gated sodium channels: Nav1.1 and Nav1.3. *Channels (Austin)*. 12:367–377. <https://doi.org/10.1080/19336950.2018.1539611>
- Ghovanloo, M.-R., N.G. Shuart, J. Mezeyova, R.A. Dean, P.C. Ruben, and S.J. Goodchild. 2018c. Inhibitory effects of cannabidiol on voltage-dependent sodium currents. *J. Biol. Chem.* 293:16546–16558. <https://doi.org/10.1074/jbc.RA118.004929>
- Ghovanloo, M.-R., J. Atallah, C.A. Escudero, and P.C. Ruben. 2020. Biophysical characterization of a novel SCN5A mutation associated with an atypical phenotype of atrial and ventricular arrhythmias and sudden death. *Front. Physiol.* 11:610436. <https://doi.org/10.3389/fphys.2020.610436>
- Hampf, M., E. Eberhardt, A.O. O'Reilly, and A. Lampert. 2016. Sodium channel slow inactivation interferes with open channel block. *Sci. Rep.* 6:25974. <https://doi.org/10.1038/srep25974>
- Harding, S.D., J.L. Sharman, E. Faccenda, C. Southan, A.J. Pawson, S. Ireland, A.J.G. Gray, L. Bruce, S.P.H. Alexander, S. Anderton, et al. NC-IUPHAR. 2018. The IUPHAR/BPS Guide to PHARMACOLOGY in 2018: updates and expansion to encompass the new guide to IMMUNOPHARMACOLOGY. *Nucleic Acids Res.* 46(D1):D1091–D1106. <https://doi.org/10.1093/nar/gkx1121>
- Heatwole, C.R., J.M. Statland, and E.L. Logigian. 2013. The diagnosis and treatment of myotonic disorders. *Muscle Nerve*. 47:632–648. <https://doi.org/10.1002/mus.23683>
- Hess, B., H. Bekker, H.J.C. Berendsen, and J.G.E.M. Fraaije. 1997. LINCS: a linear constraint solver for molecular simulations. *J. Comput. Chem.* 18: 1463–1472. [https://doi.org/10.1002/\(SICI\)1096-987X\(199709\)18:12<1463::AID-JCC4>3.0.CO;2-H](https://doi.org/10.1002/(SICI)1096-987X(199709)18:12<1463::AID-JCC4>3.0.CO;2-H)
- Hille, B. 1977. Local anesthetics: hydrophilic and hydrophobic pathways for the drug-receptor reaction. *J. Gen. Physiol.* 69:497–515. <https://doi.org/10.1085/jgp.69.4.497>
- Hille, B. 2001. Ion channels of excitable membranes. Sinauer, Sunderland, MA. 814 pp.
- Hondeghe, L.M., and B.G. Katzung. 1984. Antiarrhythmic agents: the modulated receptor mechanism of action of sodium and calcium channel-blocking drugs. *Annu. Rev. Pharmacol. Toxicol.* 24:387–423. <https://doi.org/10.1146/annurev.pa.24.040184.002131>
- Iannotti, F.A., E. Pagano, A.S. Moriello, F.G. Alvino, N.C. Sorrentino, L. D'Orsi, E. Gazzero, R. Capasso, E. De Leonibus, L. De Petrocellis, and V. Di Marzo. 2019. Effects of non-euphoric plant cannabinoids on muscle quality and performance of dystrophic mdx mice. *Br. J. Pharmacol.* 176: 1568–1584. <https://doi.org/10.1111/bph.14460>
- Ingólfsson, H.I., R.L. Sanford, R. Kapoor, and O.S. Andersen. 2010. Gramicidin-based fluorescence assay; for determining small molecules potential for modifying lipid bilayer properties. *J. Vis. Exp.* (44):2131. <https://doi.org/10.3791/2131>
- Jiang, D., T.M. Gamal El-Din, C. Ing, P. Lu, R. Pomès, N. Zheng, and W.A. Catterall. 2018. Structural basis for gating pore current in periodic paralysis. *Nature*. 557:590–594. <https://doi.org/10.1038/s41586-018-0120-4>
- Jo, S., T. Kim, V.G. Iyer, and W. Im. 2008. CHARMM-GUI: a web-based graphical user interface for CHARMM. *J. Comput. Chem.* 29:1859–1865. <https://doi.org/10.1002/jcc.20945>
- Kaplan, J.S., N. Stella, W.A. Catterall, and R.E. Westenbroek. 2017. Cannabidiol attenuates seizures and social deficits in a mouse model of Dravet syndrome. *Proc. Natl. Acad. Sci. USA*. 114:11229–11234. <https://doi.org/10.1073/pnas.1711351114>
- Kapoor, R., T.A. Peyear, R.E. Koeppe II, and O.S. Andersen. 2019. Antidepressants are modifiers of lipid bilayer properties. *J. Gen. Physiol.* 151: 342–356. <https://doi.org/10.1085/jgp.201812263>
- Khan, A.A., T. Shekh-Ahmad, A. Khalil, M.C. Walker, and A.B. Ali. 2018. Cannabidiol exerts antiepileptic effects by restoring hippocampal interneuron functions in a temporal lobe epilepsy model. *Br. J. Pharmacol.* 175:2097–2115. <https://doi.org/10.1111/bph.14202>
- Klauda, J.B., R.M. Venable, J.A. Freites, J.W. O'Connor, D.J. Tobias, C. Mondragon-Ramirez, I. Vorobyov, A.D. MacKerell Jr., and R.W. Pastor. 2010. Update of the CHARMM all-atom additive force field for lipids: validation on six lipid types. *J. Phys. Chem. B*. 114:7830–7843. <https://doi.org/10.1021/jp101759q>
- Kuo, C.C., and B.P. Bean. 1994. Slow binding of phenytoin to inactivated sodium channels in rat hippocampal neurons. *Mol. Pharmacol.* 46:716–725.
- Lafleur, M., B. Fine, E. Sternin, P.R. Cullis, and M. Bloom. 1989. Smoothed orientational order profile of lipid bilayers by ²H-nuclear magnetic resonance. *Biophys. J.* 56:1037–1041. [https://doi.org/10.1016/S0006-3495\(89\)82749-3](https://doi.org/10.1016/S0006-3495(89)82749-3)

- Laprairie, R.B., A.M. Bagher, M.E.M. Kelly, and E.M. Denovan-Wright. 2015. Cannabidiol is a negative allosteric modulator of the cannabinoid CB1 receptor. *Br. J. Pharmacol.* 172:4790–4805. <https://doi.org/10.1111/bph.13250>
- Lee, S., S.J. Goodchild, and C.A. Ahern. 2012. Local anesthetic inhibition of a bacterial sodium channel. *J. Gen. Physiol.* 139:507–516. <https://doi.org/10.1085/jgp.201210779>
- Lee, J., X. Cheng, J.M. Swails, M.S. Yeom, P.K. Eastman, J.A. Lemkul, S. Wei, J. Buckner, J.C. Jeong, Y. Qi, et al. 2016. CHARMM-GUI input generator for NAMD, GROMACS, AMBER, OpenMM, and CHARMM/OpenMM simulations using the CHARMM36 additive force field. *J. Chem. Theory Comput.* 12:405–413. <https://doi.org/10.1021/acs.jctc.5b00935>
- Lehmann-Horn, F., and R. Rüdell. 1995. Hereditary nondystrophic myotonias and periodic paralyses. *Curr. Opin. Neurol.* 8:402–410. <https://doi.org/10.1097/00019052-199510000-00014>
- Lehmann-Horn, F., K. Jurkat-Rott, and R. Rüdell. Ulm Muscle Centre. 2008. Diagnostics and therapy of muscle channelopathies--Guidelines of the Ulm Muscle Centre. *Acta Myol.* 27:98–113.
- Lundbæk, J.A., P. Birn, A.J. Hansen, R. Søgaard, C. Nielsen, J. Girshman, M.J. Bruno, S.E. Tape, J. Egebjerg, D.V. Greathouse, et al. 2004. Regulation of sodium channel function by bilayer elasticity: the importance of hydrophobic coupling. Effects of Micelle-forming amphiphiles and cholesterol. *J. Gen. Physiol.* 123:599–621. <https://doi.org/10.1085/jgp.200308996>
- Lundbæk, J.A., P. Birn, S.E. Tape, G.E. Toombs, R. Søgaard, R.E. Koeppe II, S.M. Gruner, A.J. Hansen, and O.S. Andersen. 2005. Capsaicin regulates voltage-dependent sodium channels by altering lipid bilayer elasticity. *Mol. Pharmacol.* 68:680–689. <https://doi.org/10.1124/mol.105.013573>
- Lundbæk, J.A., S.A. Collingwood, H.I. Ingólfsson, R. Kapoor, and O.S. Andersen. 2010. Lipid bilayer regulation of membrane protein function: gramicidin channels as molecular force probes. *J. R. Soc. Interface.* 7: 373–395. <https://doi.org/10.1098/rsif.2009.0443>
- Mantegazza, M., G. Curia, G. Biagini, D.S. Ragsdale, and M. Avoli. 2010. Voltage-gated sodium channels as therapeutic targets in epilepsy and other neurological disorders. *Lancet Neurol.* 9:413–424. [https://doi.org/10.1016/S1474-4422\(10\)70059-4](https://doi.org/10.1016/S1474-4422(10)70059-4)
- Marchi, M., and P. Ballone. 1999. Adiabatic bias molecular dynamics: a method to navigate the conformational space of complex molecular systems. *J. Chem. Phys.* 110:3697–3702. <https://doi.org/10.1063/1.478259>
- Miller, T.M., M.R. Dias da Silva, H.A. Miller, H. Kwiecinski, J.R. Mendell, R. Tawil, P. McManis, R.C. Griggs, C. Angelini, S. Servidei, et al. 2004. Correlating phenotype and genotype in the periodic paralyses. *Neurology.* 63:1647–1655. <https://doi.org/10.1212/01.WNL.0000143383.91137.00>
- Morales, P., D.P. Hurst, and P.H. Reggio. 2017. Molecular targets of the phytocannabinoids: a complex picture. *Prog. Chem. Org. Nat. Prod.* 103: 103–131.
- Nosé, S. 1984. A unified formulation of the constant temperature molecular dynamics methods. *J. Chem. Phys.* 81:511–519. <https://doi.org/10.1063/1.447334>
- Nuss, H.B., G.F. Tomaselli, and E. Marbán. 1995. Cardiac sodium channels (hH1) are intrinsically more sensitive to block by lidocaine than are skeletal muscle (μ 1) channels. *J. Gen. Physiol.* 106:1193–1209. <https://doi.org/10.1085/jgp.106.6.1193>
- O'Connell, A.M., R.E. Koeppe II, and O.S. Andersen. 1990. Kinetics of gramicidin channel formation in lipid bilayers: transmembrane monomer association. *Science.* 250:1256–1259. <https://doi.org/10.1126/science.1700867>
- Pan, X., Z. Li, Q. Zhou, H. Shen, K. Wu, X. Huang, J. Chen, J. Zhang, X. Zhu, J. Lei, et al. 2018. Structure of the human voltage-gated sodium channel $\text{Na}_v1.4$ in complex with β 1. *Science.* 362:eaau2486. <https://doi.org/10.1126/science.aau2486>
- Parrinello, M., and A. Rahman. 1981. Polymorphic transitions in single crystals: a new molecular dynamics method. *J. Appl. Phys.* 52:7182–7190. <https://doi.org/10.1063/1.328693>
- Patel, R.R., C. Barbosa, T. Brustovetsky, N. Brustovetsky, and T.R. Cummins. 2016. Aberrant epilepsy-associated mutant $\text{Nav}1.6$ sodium channel activity can be targeted with cannabidiol. *Brain.* 139:2164–2181. <https://doi.org/10.1093/brain/aww129>
- Pertwee, R.G. 2008. The diverse CB1 and CB2 receptor pharmacology of three plant cannabinoids: delta9-tetrahydrocannabinol, cannabidiol and delta9-tetrahydrocannabinol. *Br. J. Pharmacol.* 153:199–215. <https://doi.org/10.1038/sj.bjp.0707442>
- Peters, C.H., M.-R. Ghovanloo, C. Gershon, and P.C. Ruben. 2018. pH modulation of voltage-gated sodium channels. *Handb. Exp. Pharmacol.* 246:147–160.
- Pumroy, R.A., A. Samanta, Y. Liu, T.E. Hughes, S. Zhao, Y. Yudin, T. Rohacs, S. Han, and V.Y. Moiseenkova-Bell. 2019. Molecular mechanism of TRPV2 channel modulation by cannabidiol. *eLife.* 8:e48792. <https://doi.org/10.7554/eLife.48792>
- Richmond, J.E., D.E. Featherstone, H.A. Hartmann, and P.C. Ruben. 1998. Slow inactivation in human cardiac sodium channels. *Biophys. J.* 74: 2945–2952. [https://doi.org/10.1016/S0006-3495\(98\)78001-4](https://doi.org/10.1016/S0006-3495(98)78001-4)
- Ross, H.R., I. Napier, and M. Connor. 2008. Inhibition of recombinant human T-type calcium channels by Δ^9 -tetrahydrocannabinol and cannabidiol. *J. Biol. Chem.* 283:16124–16134. <https://doi.org/10.1074/jbc.M707104200>
- Rusinova, R., K.F. Herold, R.L. Sanford, D.V. Greathouse, H.C. Hemmings Jr., and O.S. Andersen. 2011. Thiazolidinedione insulin sensitizers alter lipid bilayer properties and voltage-dependent sodium channel function: implications for drug discovery. *J. Gen. Physiol.* 138:249–270. <https://doi.org/10.1085/jgp.201010529>
- Rusinova, R., R.E. Koeppe II, and O.S. Andersen. 2015. A general mechanism for drug promiscuity: Studies with amiodarone and other antiarrhythmics. *J. Gen. Physiol.* 146:463–475. <https://doi.org/10.1085/jgp.201511470>
- Sait, L.G., A. Sula, M.-R. Ghovanloo, D. Hollingworth, P.C. Ruben, and B.A. Wallace. 2020. Cannabidiol interactions with voltage-gated sodium channels. *eLife.* 9:e58593. <https://doi.org/10.7554/eLife.58593>
- Sokolov, S., C.H. Peters, S. Rajamani, and P.C. Ruben. 2013. Proton-dependent inhibition of the cardiac sodium channel $\text{Nav}1.5$ by ranolazine. *Front. Pharmacol.* 4:78. <https://doi.org/10.3389/fphar.2013.00078>
- Starmer, C.F., A.O. Grant, and H.C. Strauss. 1984. Mechanisms of use-dependent block of sodium channels in excitable membranes by local anesthetics. *Biophys. J.* 46:15–27. [https://doi.org/10.1016/S0006-3495\(84\)83994-6](https://doi.org/10.1016/S0006-3495(84)83994-6)
- Sternberg, D., T. Maisonobe, K. Jurkat-Rott, S. Nicole, E. Launay, D. Chauveau, N. Tabti, F. Lehmann-Horn, B. Hainque, and B. Fontaine. 2001. Hypokalaemic periodic paralysis type 2 caused by mutations at codon 672 in the muscle sodium channel gene $\text{SCN}4\text{A}$. *Brain.* 124:1091–1099. <https://doi.org/10.1093/brain/124.6.1091>
- Tan, S.V., E. Matthews, M. Barber, J.A. Burge, S. Rajakulendran, D. Fialho, R. Sud, A. Haworth, M. Koltzenburg, and M.G. Hanna. 2011. Refined exercise testing can aid DNA-based diagnosis in muscle channelopathies. *Ann. Neurol.* 69:328–340. <https://doi.org/10.1002/ana.22238>
- Tanabe, T., A. Mikami, T. Niidome, S. Numa, B.A. Adams, and K.G. Beam. 1993. Structure and function of voltage-dependent calcium channels from muscle. *Ann. N. Y. Acad. Sci.* 707(1 Molecular Bas):81–86. <https://doi.org/10.1111/j.1749-6632.1993.tb38044.x>
- Tawil, R., M.P. McDermott, R. Brown Jr., B.C. Shapiro, L.J. Ptacek, P.G. McManis, M.C. Dalakas, S.A. Spector, J.R. Mendell, A.F. Hahn, and R.C. Griggs. Working Group on Periodic Paralysis. 2000. Randomized trials of dichlorphenamide in the periodic paralyses. *Ann. Neurol.* 47:46–53. [https://doi.org/10.1002/1531-8249\(200001\)47:1<46::AID-ANA9>3.0.CO;2-H](https://doi.org/10.1002/1531-8249(200001)47:1<46::AID-ANA9>3.0.CO;2-H)
- Tham, M., O. Yilmaz, M. Alaverdashvili, M.E.M. Kelly, E.M. Denovan-Wright, and R.B. Laprairie. 2019. Allosteric and orthosteric pharmacology of cannabidiol and cannabidiol-dimethylheptyl at the type 1 and type 2 cannabinoid receptors. *Br. J. Pharmacol.* 176:1455–1469. <https://doi.org/10.1111/bph.14440>
- Thomas, A., G.L. Baillie, A.M. Phillips, R.K. Razdan, R.A. Ross, and R.G. Pertwee. 2007. Cannabidiol displays unexpectedly high potency as an antagonist of CB_1 and CB_2 receptor agonists *in vitro*. *Br. J. Pharmacol.* 150: 613–623. <https://doi.org/10.1038/sj.bjp.0707133>
- Tombola, F., M.M. Pathak, and E.Y. Isacoff. 2005. Voltage-sensing arginines in a potassium channel permeate and occlude cation-selective pores. *Neuron.* 45:379–388. <https://doi.org/10.1016/j.neuron.2004.12.047>
- Torres, C.F., R.C. Griggs, R.T. Moxley, and A.N. Bender. 1981. Hypokalemic periodic paralysis exacerbated by acetazolamide. *Neurology.* 31: 1423–1428. <https://doi.org/10.1212/WNL.31.11.1423>
- Tribello, G.A., M. Bonomi, D. Branduardi, C. Camilloni, and G. Bussi. 2014. PLUMED 2: new feathers for an old bird. *Comput. Phys. Commun.* 185: 604–613. <https://doi.org/10.1016/j.cpc.2013.09.018>
- Trip, J., G. Drost, D.J. Verbove, A.J. van der Kooij, J.B.M. Kuks, N.C. Notermans, J.J. Verschuuren, M. de Visser, B.G.M. van Engelen, C.G. Faber, and I.B. Ginjaar. 2008. In tandem analysis of CLCN1 and $\text{SCN}4\text{A}$ greatly enhances mutation detection in families with non-dystrophic myotonia. *Eur. J. Hum. Genet.* 16:921–929. <https://doi.org/10.1038/ejhg.2008.39>
- Trott, O., and A.J. Olson. 2010. AutoDock Vina: improving the speed and accuracy of docking with a new scoring function, efficient optimization, and multithreading. *J. Comput. Chem.* 31:455–461. <https://doi.org/10.1002/jcc.21334>

- Venance, S.L., K. Jurkat-Rott, F. Lehmann-Horn, and R. Tawil. 2004. SCN4A-associated hypokalemic periodic paralysis merits a trial of acetazolamide. *Neurology*. 63:1977. <https://doi.org/10.1212/01.WNL.0000143068.99794.5B>
- Vicart, S., D. Sternberg, B. Fontaine, and G. Meola. 2005. Human skeletal muscle sodium channelopathies. *Neurol. Sci.* 26:194–202. <https://doi.org/10.1007/s10072-005-0461-x>
- Webb, J., and S.C. Cannon. 2008. Cold-induced defects of sodium channel gating in atypical periodic paralysis plus myotonia. *Neurology*. 70: 755–761. <https://doi.org/10.1212/01.wnl.0000265397.70057.d8>
- Williams, S.R., S.R. Christensen, G.J. Stuart, and M. Häusser. 2002. Membrane potential bistability is controlled by the hyperpolarization-activated current $I_{(H)}$ in rat cerebellar Purkinje neurons *in vitro*. *J. Physiol.* 539:469–483. <https://doi.org/10.1113/jphysiol.2001.013136>
- Wishart, D.S., Y.D. Feunang, A.C. Guo, E.J. Lo, A. Marcu, J.R. Grant, T. Sajed, D. Johnson, C. Li, Z. Sayeeda, et al. 2018. DrugBank 5.0: a major update to the DrugBank database for 2018. *Nucleic Acids Res.* 46(D1): D1074–D1082. <https://doi.org/10.1093/nar/gkx1037>
- Wu, F., W. Mi, D.K. Burns, Y. Fu, H.F. Gray, A.F. Struyk, and S.C. Cannon. 2011. A sodium channel knockin mutant (Nav1.4-R669H) mouse model of hypokalemic periodic paralysis. *J. Clin. Invest.* 121:4082–4094. <https://doi.org/10.1172/JCI57398>
- Wu, E.L., X. Cheng, S. Jo, H. Rui, K.C. Song, E.M. Dávila-Contreras, Y. Qi, J. Lee, V. Monje-Galvan, R.M. Venable, et al. 2014. CHARMM-GUI Membrane Builder toward realistic biological membrane simulations. *J. Comput. Chem.* 35:1997–2004. <https://doi.org/10.1002/jcc.23702>
- Yarov-Yarovoy, V., P.G. DeCaen, R.E. Westenbroek, C.-Y. Pan, T. Scheuer, D. Baker, and W.A. Catterall. 2012. Structural basis for gating charge movement in the voltage sensor of a sodium channel. *Proc. Natl. Acad. Sci. USA.* 109:E93–E102. <https://doi.org/10.1073/pnas.1118434109>
- Zoete, V., M.A. Cuendet, A. Grosdidier, and O. Michielin. 2011. SwissParam: a fast force field generation tool for small organic molecules. *J. Comput. Chem.* 32:2359–2368. <https://doi.org/10.1002/jcc.21816>

Supplemental material

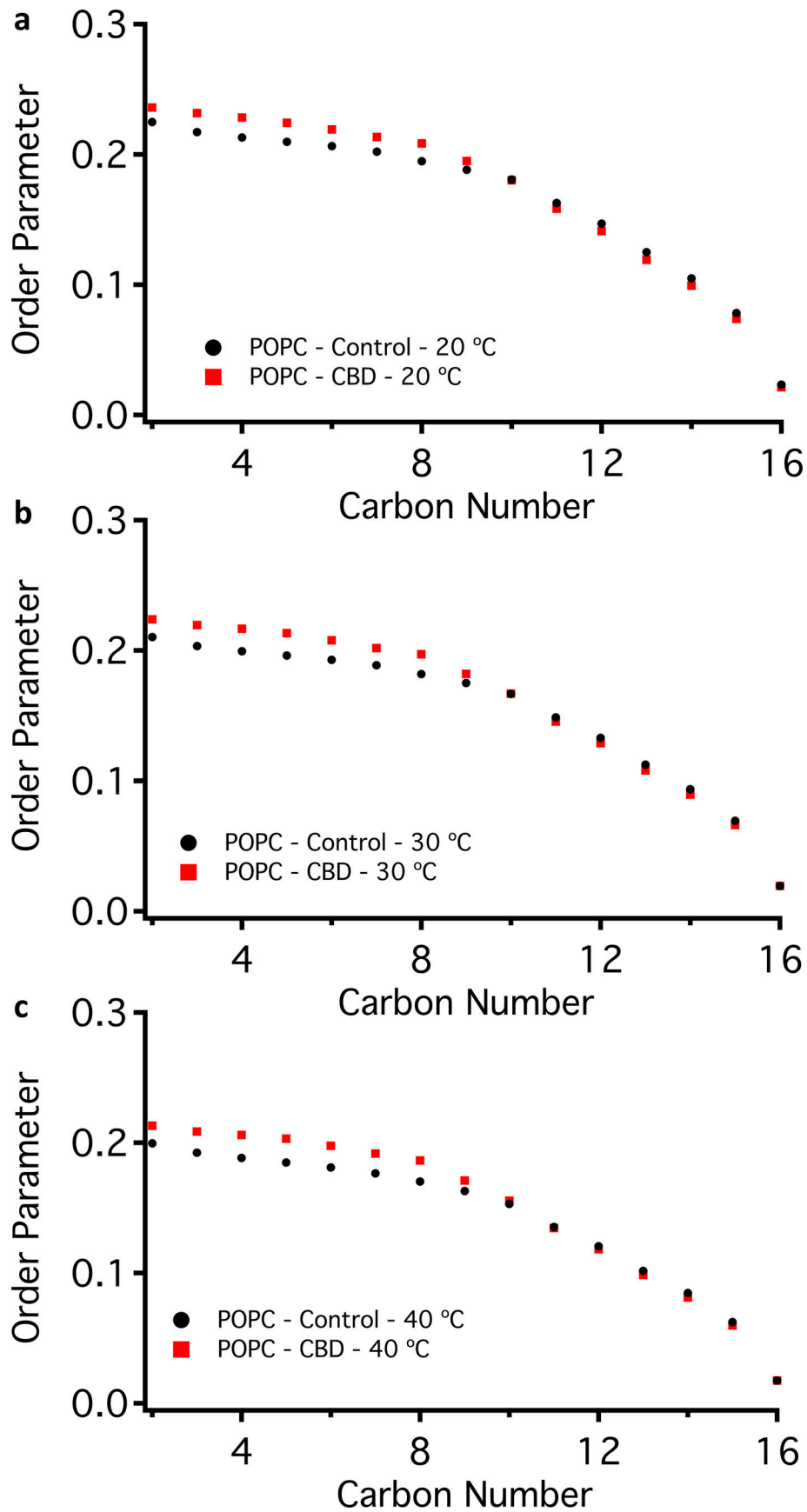
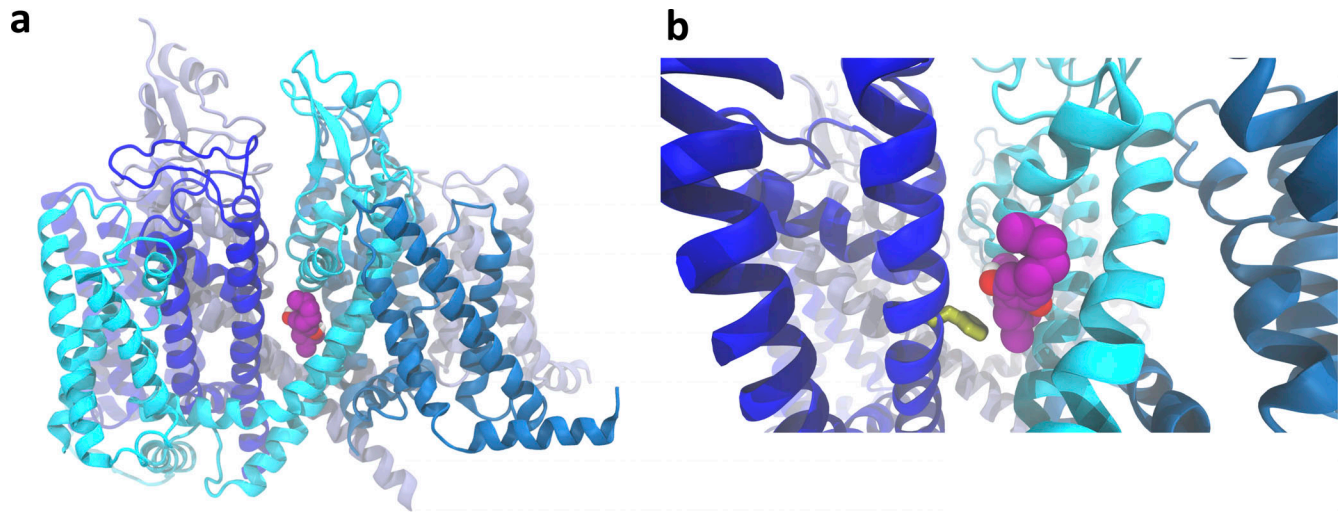
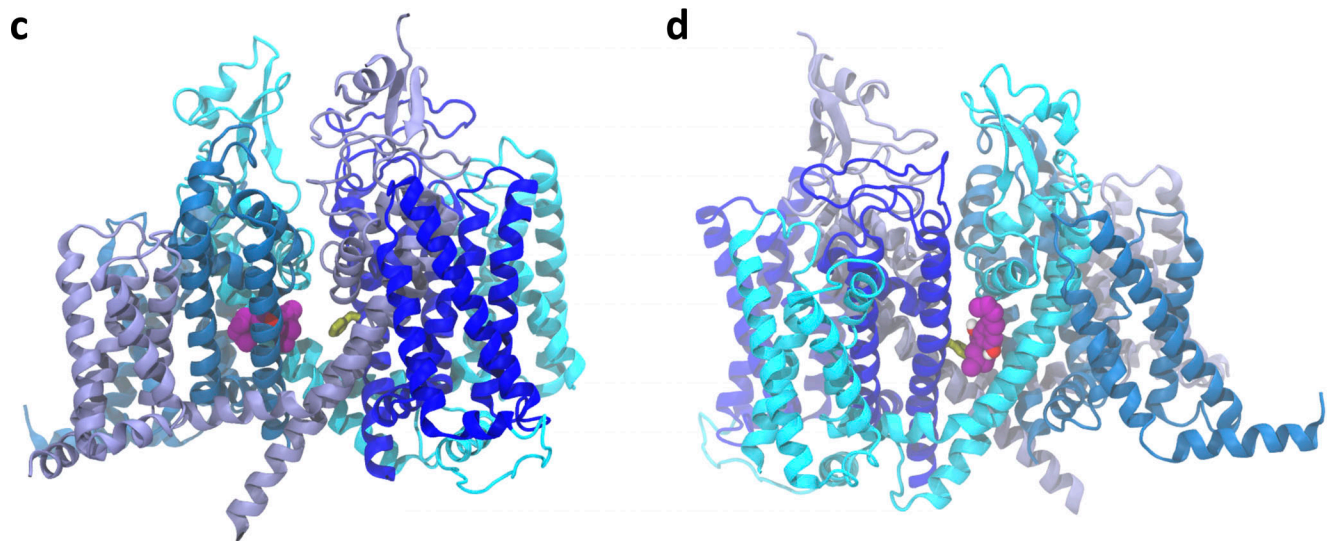


Figure S1. ^2H NMR at different temperatures and further characterization of F1586A. (a-c) Order parameters associated with POPC membranes at 20°C (a), 30°C (b), and 40°C (c).



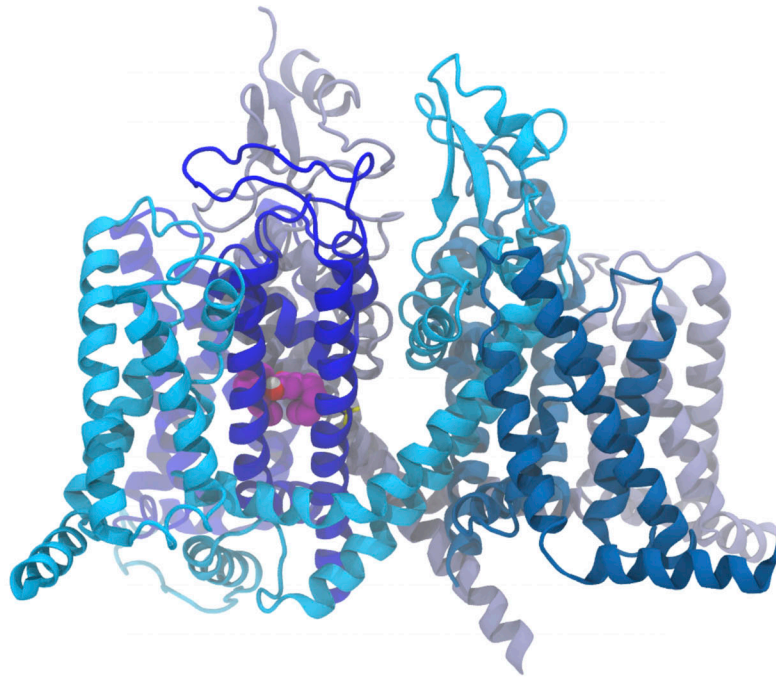
CBD in hNav1.4 (PDB ID – 6AGF) in the best position energy wise (-7.9 kcal/mol)



CBD in hNav1.4 (PDB ID – 6AGF) in the second and third best position energy wise (-7.8 kcal/mol)

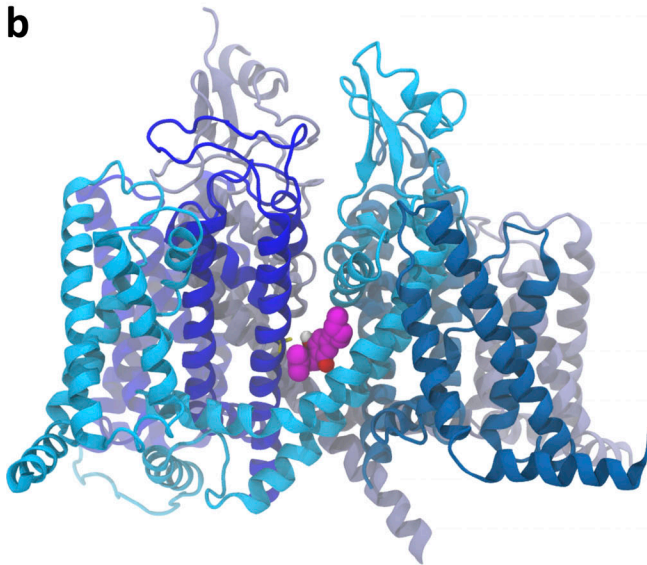
Figure S2. **Nav1.4 WT interactions with CBD.** (a-d) CBD posed in the human Nav1.4 structure using molecular docking.

a

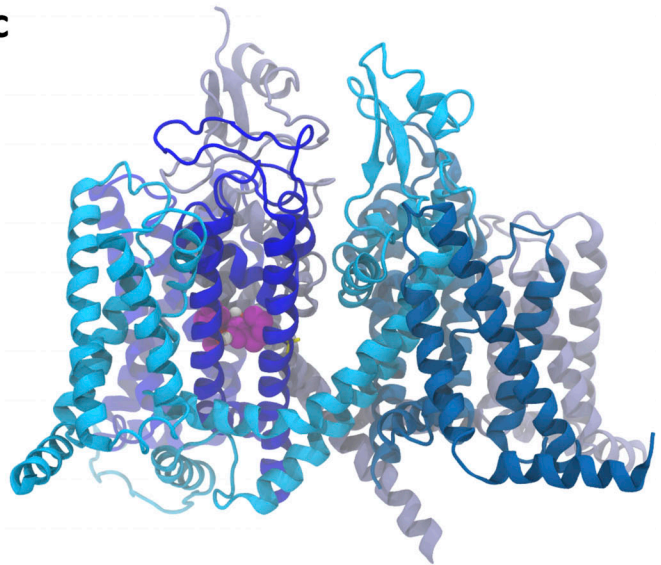


CBD in hNav1.4 (PDB ID – 6AGF) in the best position energy wise (-7.6 kcal/mol)

b



c



CBD in hNav1.4 (PDB ID – 6AGF) in the second and third best position energy wise (-7.6 and -7.5 kcal/mol, respectively)

Figure S3. **Nav1.4 F1586A interactions with CBD.** (a-c) CBD posed in the human Nav1.4 structure using molecular docking.

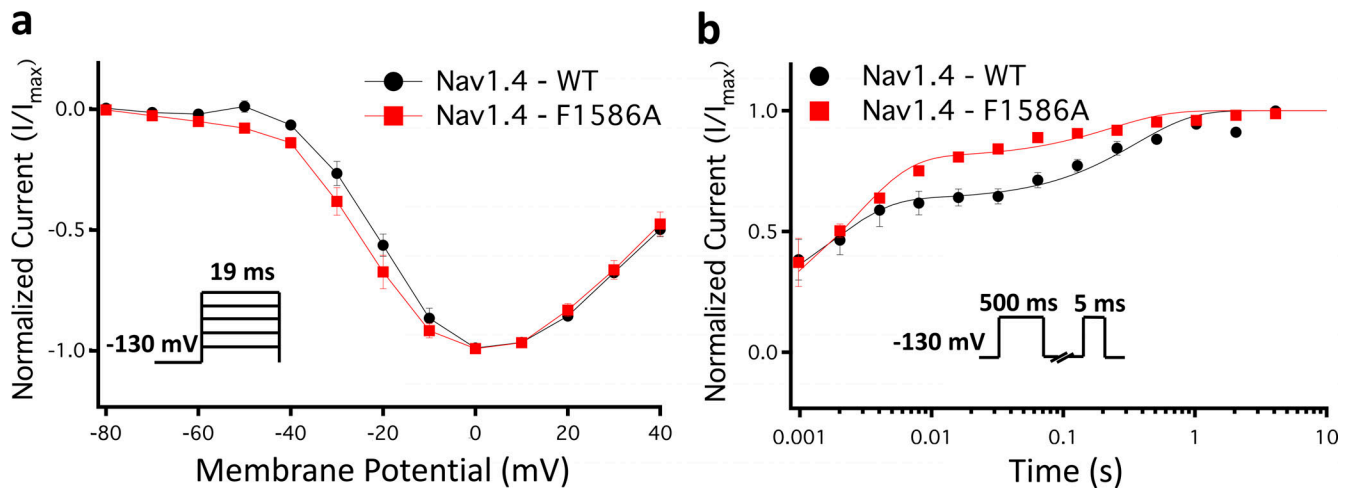


Figure S4. **Further characterization of F1586A.** (a and b) Normalized activating currents as a function of potential, recovery from fast inactivation (Nav1.4: $\tau_{Fast} = 0.0025 \pm 0.00069$ s, $\tau_{Slow} = 0.224 \pm 0.046$ s, $n = 7$; F1586A: $\tau_{Fast} = 0.0021 \pm 0.00043$ s; $\tau_{Slow} = 0.093718 \pm 0.03673$ s, $n = 6$; $P > 0.05$ for τ_{Fast} and $P = 0.0250$ for τ_{Slow}).

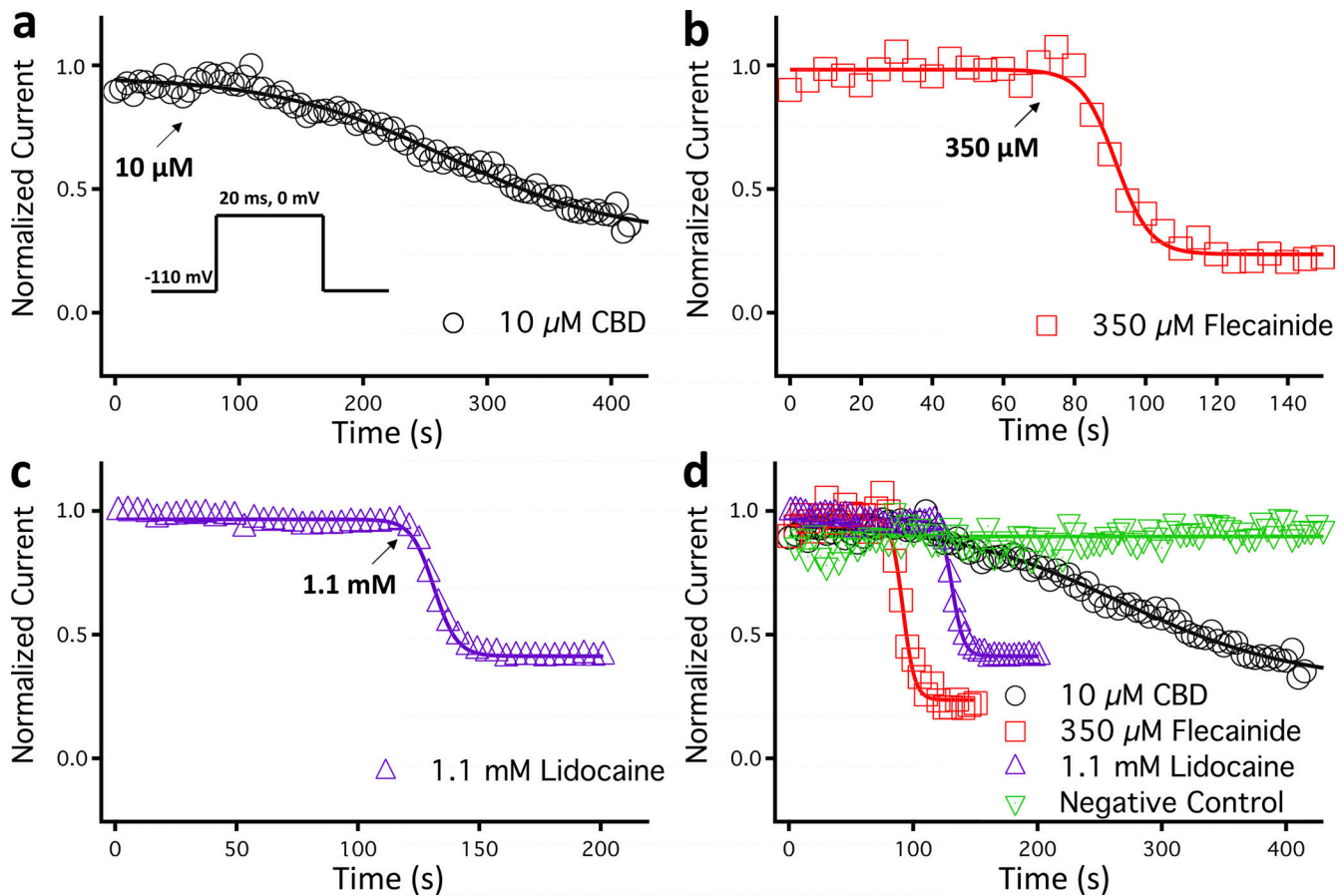


Figure S5. **Sample normalized time dependence.** (a-d) Time dependence of CBD (70.5 ± 6.9 s), flecainide (4.8 ± 0.7 s), lidocaine (4.7 ± 0.2 s), and negative control (no compound). Error bars are SE in mean.

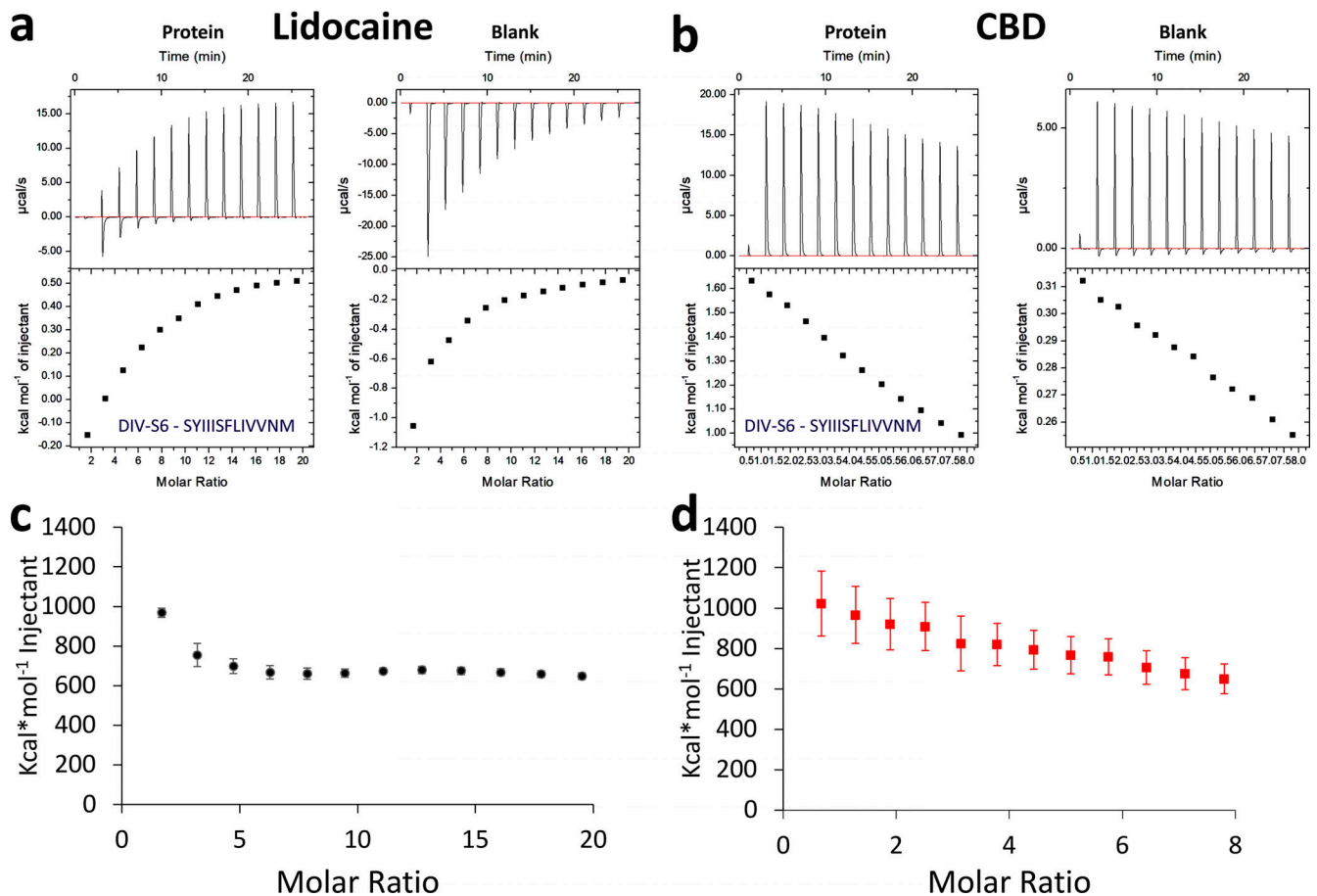


Figure S6. **CBD interactions with DIV-S6, using ITC.** (a) Representative ITC traces for titration of 100 mM lidocaine into 1 mM peptide or blank buffer. The heat signal, once the binding is saturated is the same as the blank if the blank was only measuring the interaction of lidocaine with the solution. The blank measures 3 interactions, interactions between solute molecules, solute and lidocaine and lidocaine and lidocaine. As more lidocaine is added with each injection the solution is changed. This makes the heat of interaction with in-blank trace different from beginning to end. This change is due to a change in amount of lidocaine in the solution. Because this change is progressive with each injection and that the injections into the peptide are the same volume, subtraction was used as a means to quantify lidocaine peptide interaction. (b) Representative ITC traces for titration of 40 mM CBD into 1 mM peptide or blank buffer. (c and d) The blank condition subtracted heat of titration in protein condition is shown for lidocaine (c) and CBD (d). A peak heat of 968.0 ± 23.4 kcal mol⁻¹ was seen for lidocaine ($n = 3$) titration, and a peak heat of $1,022.2 \pm 160.6$ kcal mol⁻¹ was seen for the CBD ($n = 4$) titration. Error bars are SE in mean.

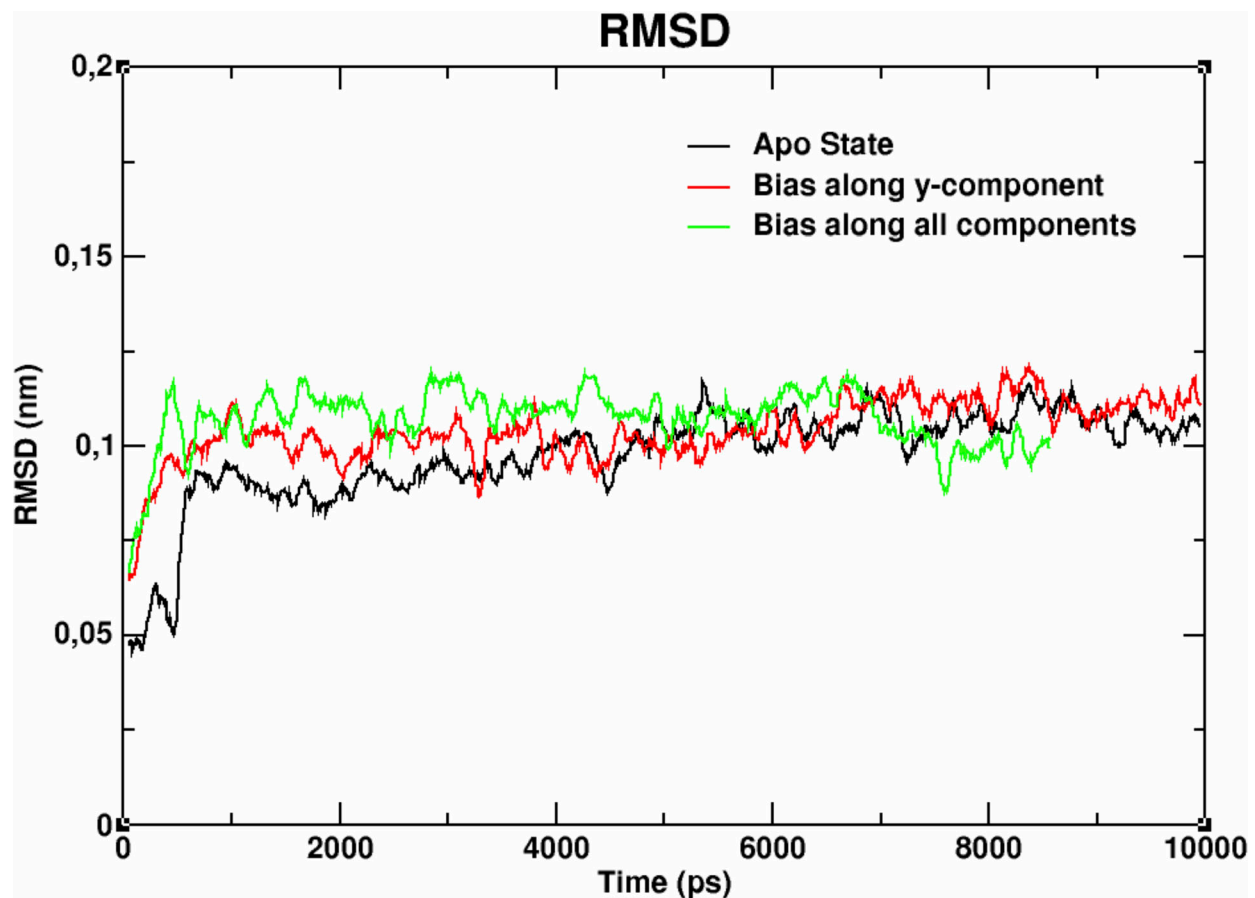


Figure S7. **Structural integrity MD simulation of CBD pathway through the Nav1.4 fenestration.** Root mean square deviation (RMSD) of the fenestration residues as a function of time in the absence (black) and the presence of CBD passing through the fenestration (red and green, two different simulation parameter sets). Apo means unbound in the absence of CBD. The similar RMSD profiles show that CBD's passage does not distort the structural integrity of the fenestration.

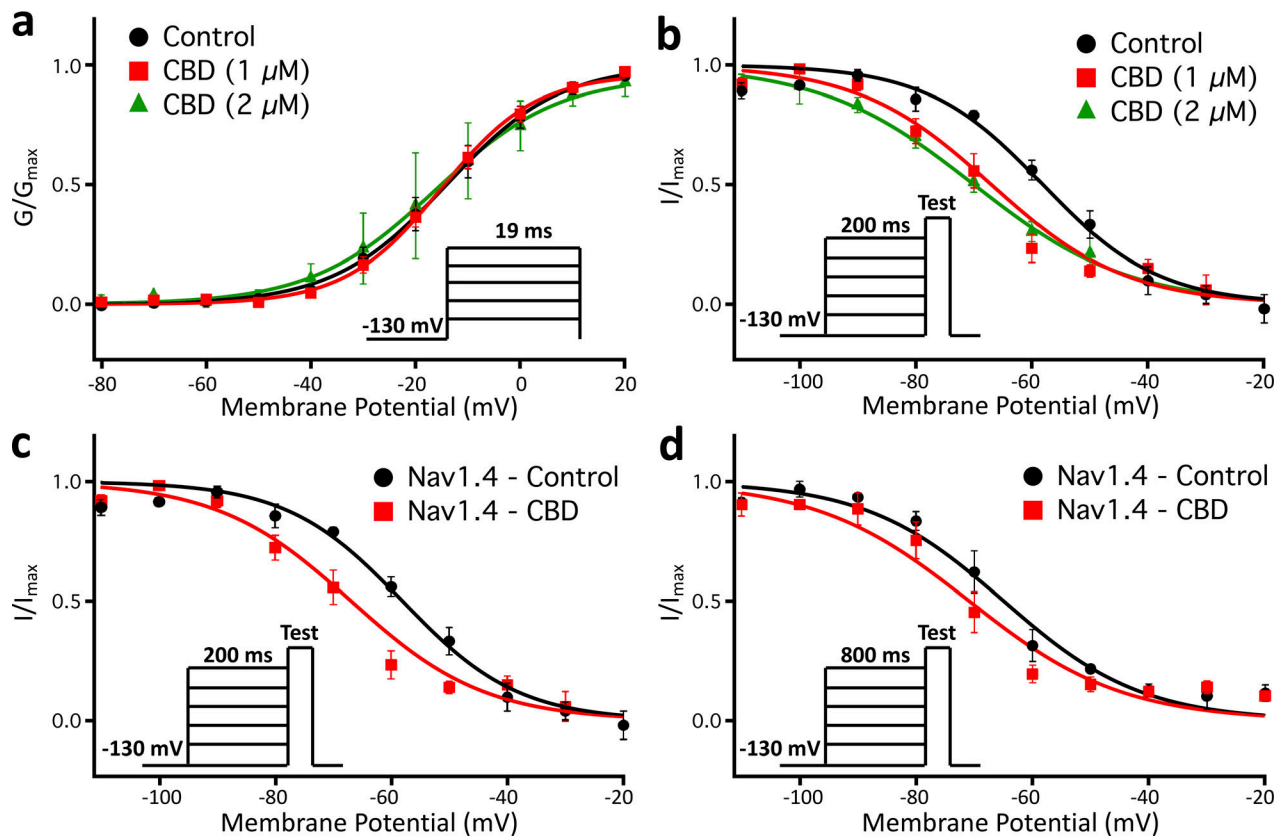


Figure S8. **CBD concentration dependence and varying pulse duration F-I curve measurement. (a and b)** Show voltage dependence of activation (control: -19.9 ± 4.2 mV, $z = 2.8 \pm 0.3$, $n = 5$; $1 \mu\text{M}$: $V_{1/2} = -14.3 \pm 4.2$ mV, $z = 2.8 \pm 0.3$, $n = 5$; $2 \mu\text{M}$: $V_{1/2} = -21.2 \pm 8.1$ mV, $z = 3.2 \pm 0.4$, $n = 4$; $P > 0.05$ for both $V_{1/2}$ and z for both 1 and $2 \mu\text{M}$ CBD) and 200 -ms F-I curve (control: $V_{1/2} = -64.1 \pm 2.4$ mV, $z = -2.7 \pm 0.3$, $n = 8$; $1 \mu\text{M}$: $V_{1/2} = -72.7 \pm 3.0$ mV, $z = -2.8 \pm 0.4$, $n = 5$; $2 \mu\text{M}$: $V_{1/2} = -75.5 \pm 0.8$ mV, $z = -2.2 \pm 0.5$, $n = 3$; $P = 0.0281$ for $V_{1/2}$ and $P > 0.05$ for z [$1 \mu\text{M}$] and $P = 0.0073$ for $V_{1/2}$ and $P > 0.05$ for z [$2 \mu\text{M}$]) at 0 , 1 , and $2 \mu\text{M}$ CBD. Statistical tests were performed for either CBD concentrations against control/ $0 \mu\text{M}$ CBD. **(c and d)** Voltage dependence of F-I curve from 200 ms (control: $V_{1/2} = -64.1 \pm 2.4$ mV, $z = -2.7 \pm 0.3$, $n = 8$; CBD $1 \mu\text{M}$: $V_{1/2} = -72.7 \pm 3.0$ mV, $z = -2.8 \pm 0.4$, $n = 5$; $P = 0.0281$ for $V_{1/2}$ and $P > 0.05$ for z) and 800 ms (control: $V_{1/2} = -64.9 \pm 1.2$ mV, $z = -2.1 \pm 0.2$, $n = 4$; CBD $1 \mu\text{M}$: $V_{1/2} = -70.9 \pm 1.3$ mV, $z = -1.9 \pm 0.2$, $n = 4$; $P < 0.05$ for $V_{1/2}$ and $P > 0.05$ for z).

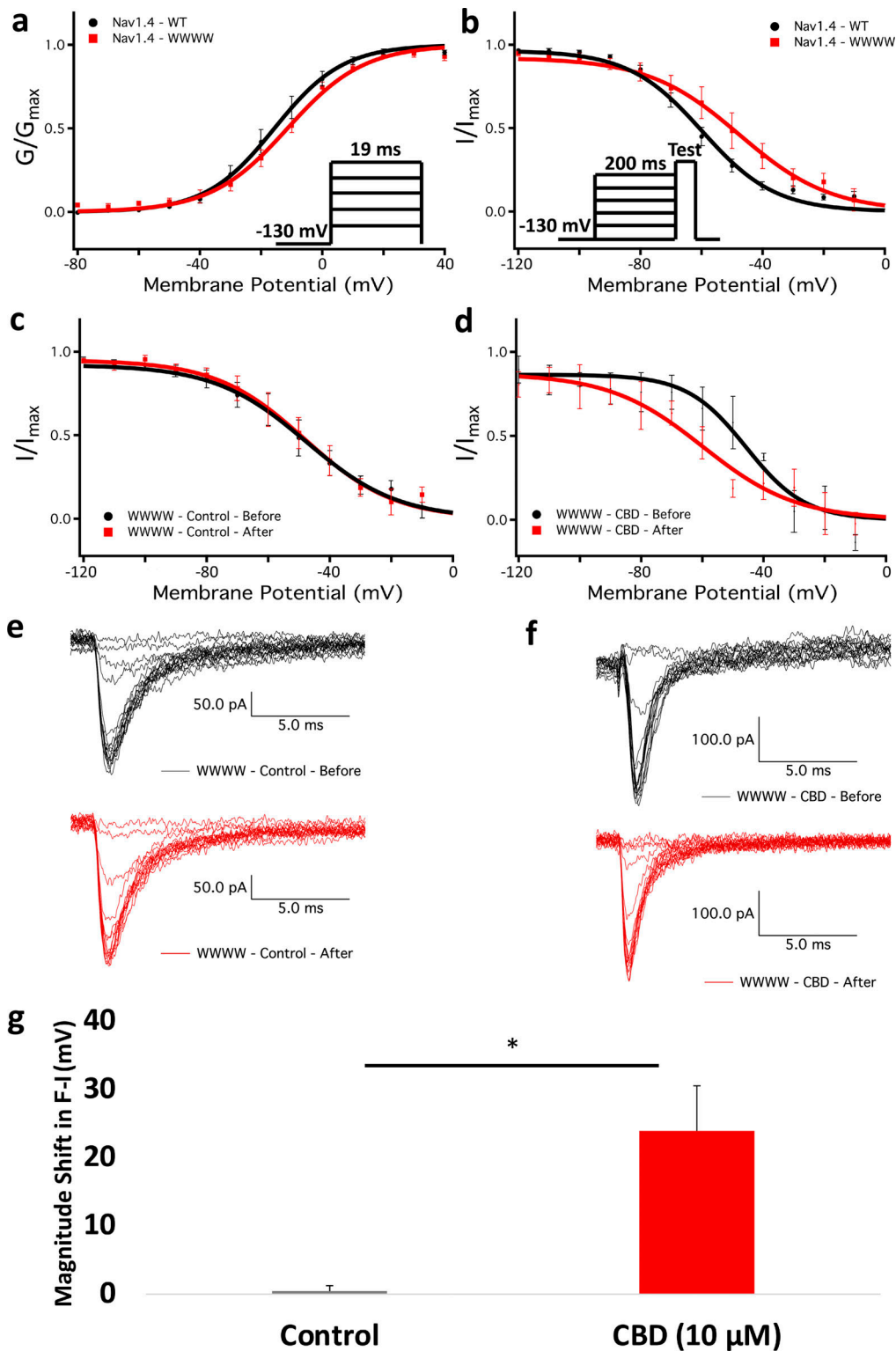


Figure S9. **WWWW characterization; CBD stabilizes inactivation in the fenestration-altered construct.** (a and b) Conductance voltage (GV) of the construct compared with WT-Nav1.4 (Nav1.4: $V_{1/2} = -19.9 \pm 2.7$ mV, $z = 2.8 \pm 0.3$, $n = 5$; WWWW: $V_{1/2} = -11.4 \pm 0.4$ mV, $z = 2.0 \pm 0.1$; $P = 0.0113$ for $V_{1/2}$ and $P > 0.05$ for z , $n = 7$) and 200-ms F-I curve (Nav1.4: $V_{1/2} = -64.1 \pm 2.4$ mV, $z = -2.7 \pm 0.3$, $n = 8$; WWWW: $V_{1/2} = -47.6 \pm 0.5$ mV, $z = 1.7 \pm 0.04$, $n = 5$; $P < 0.05$ for both $V_{1/2}$ and z). Both channels are full availability at -110 mV. (c and d) Voltage dependence of 200-ms F-I curve before and after control (c; extracellular solution [ECS]) and CBD (d; 10 μ M) in WWWW construct (before control: $V_{1/2} = -54.7 \pm 5.1$ mV, $n = 6$; after control: $V_{1/2} = -54.2 \pm 5.4$ mV, $n = 6$; before CBD: $V_{1/2} = -48.8 \pm 8.8$ mV, $n = 3$; after CBD: $V_{1/2} = -72.7 \pm 5.7$ mV, $n = 3$, $P = 0.0068$ for CBD in matched-pair analysis). The ECS experiment was performed to ensure that hyperpolarization shifts in the CBD condition are not due to possible confounding effects associated with fluoride in the internal (CsF) solutions. (e and f) Representative families of inactivating currents before and after perfusion. CBD does not block peak currents but shifts the F-I curve to the left. (g) Averaged shift in the midpoint of F-I curve before and after perfusion. *, $P < 0.05$. Error bars are SE in mean.

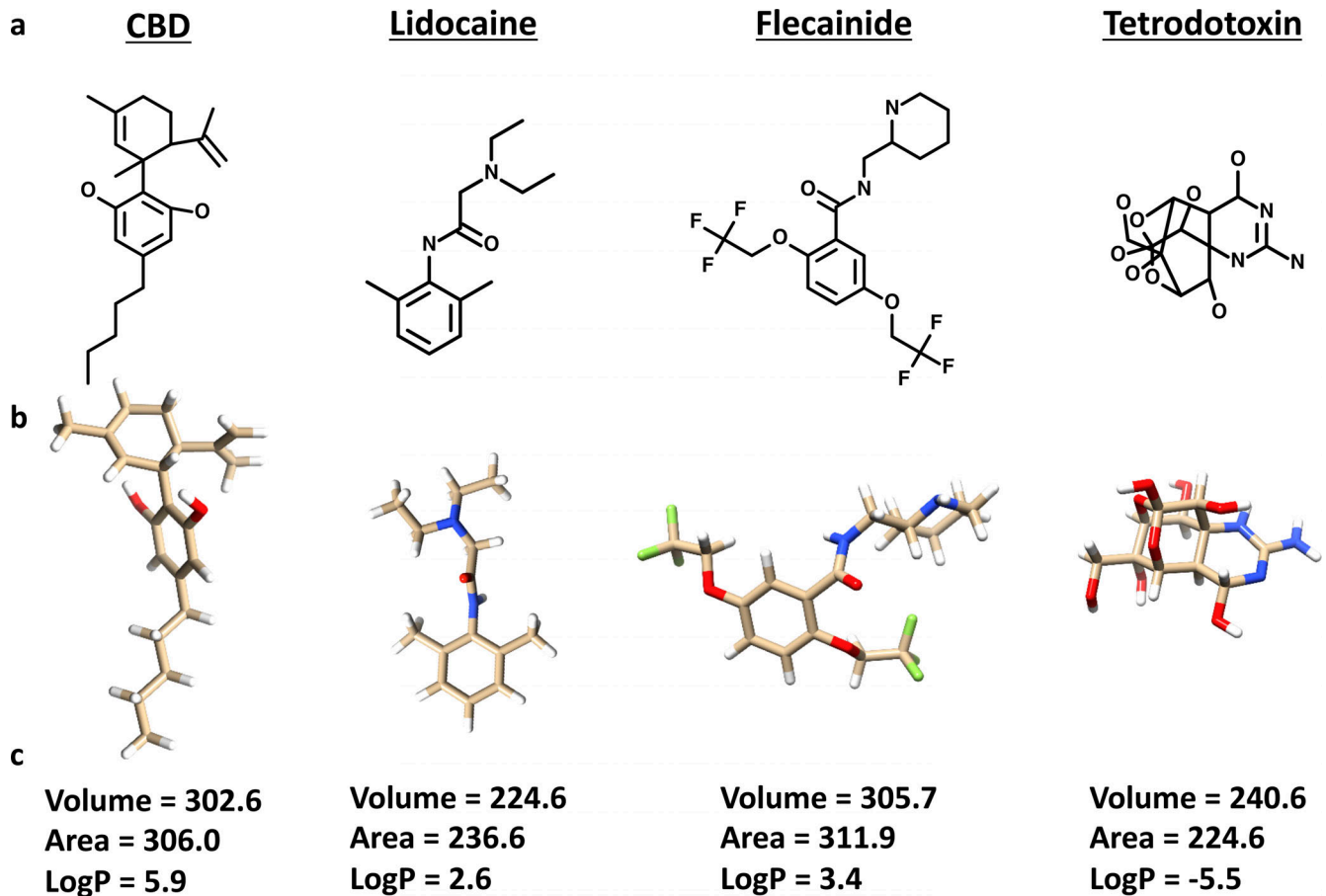


Figure S10. **Comparison between some of the relevant physicochemical properties of the compounds used in this study.** (a) Chemical structures of the compounds used in this study. (b) 3-D structures of the compounds. (c) Volume (\AA^3) and area (\AA^2) for each compound were calculated using University of California, San Francisco Chimera. LogP values are obtained from the ChEMBL database. CBD, lidocaine, and flecainide all interact with the LA site inside the Nav pore. TTX interacts with the outer selectivity filter of the Nav pore. CBD is several times more hydrophobic than the other compounds. CBD is larger than lidocaine and slightly smaller than flecainide.

Video 1. **CBD localization inside POPC membrane.** Playback speed ~79 frames/s.

Video 2. **ABMD simulation shows that CBD passes through the fenestration of Nav1.4 (bias applied along y component of distance).** Playback speed 33 frames/s.

Video 3. **ABMD simulation shows that CBD passes through the fenestration of Nav1.4 (bias applied along all components of distance).** Playback speed 25 frames/s.

Provided online are three tables. Table S1 shows data comparing CBD inhibition of Nav1.4 at two different frequencies. Table S2 lists details of the MD simulation systems. Table S3 lists numbers associated with AP modeling.